

Control of Multipartite Entanglement through Anisotropy against Thermal Noise

Samudra Sur^{1,*} and Saikat Sur^{2,†}

¹Department of Quantum Matter Physics, University of Geneva, Quai Ernest-Ansermet 24, 1211 Geneva, Switzerland

²Optics & Quantum Information Group, The Institute of Mathematical Sciences, HBNI, CIT Campus, Taramani, Chennai 600113, India

Preserving multipartite entanglement in open many-body quantum systems is fundamentally limited by unavoidable environmental noise. We study the open-system dynamics of multipartite entanglement in an anisotropic XXZ spin chain interacting with a thermal spin bath, focusing on two states with distinct types of multipartite entanglement: the generalized Greenberger–Horne–Zeilinger and the generalized W state. Using a master-equation approach combined with the Bethe ansatz technique, we show analytically that robustness of multipartite entanglement at low temperatures can be enhanced by suitably tuning the anisotropy of the system. Our results highlight interaction-induced spectral control as a mechanism for stabilizing multipartite entanglement in quantum computing platforms.

A long-standing challenge in the development of quantum devices is preserving a quantum state with entanglement in a many-body system, as complete isolation from the environment is practically unattainable [1–3]. In a many-body quantum system, *multipartite entanglement* serves as a key resource for tasks like quantum secret sharing [4–7], quantum key distribution [8, 9], multiparty quantum teleportation [10, 11], quantum metrology [12], measurement-based quantum computation [13, 14], quantum error-correction [15, 16]. Among the paradigmatic genuinely multipartite entangled states, the Greenberger–Horne–Zeilinger (GHZ) and the W state represent two inequivalent classes of resource states that are distinct under local operations and classical communication (LOCC) [9]. However, initially pure states are prone to decoherence and turn into mixed states due to environmental couplings.

A generic mixed state is said to possess genuine multipartite entanglement (GME) if it cannot be expressed as a mixture of states that are separable across any bipartition [18, 19]. However, in large many-body systems, quantification of GME is challenging as the number of bipartitions grows exponentially with system size [6, 20]. In the continuum limit, GME could become non-computable due to diverging or non-normalizable entanglement measures [21]. Furthermore, unlike bipartite entanglement, GME does not have a unique quantitative measure for mixed states [7]. To overcome these difficulties, the *distillation fraction* of a chosen reference family of resource states can serve as a quantitative marker of GME in many-body systems [22, 23]. The distillation fraction measures the asymptotic fraction of copies that can be converted into the reference resource state given many copies of a state and a set of allowed local operations. On the other hand, for Dicke type entangled states, the GME measures often become non-extensive. In such cases, we employ the geometric measure of collective multipartite entanglement (CME) defined with respect to the set of fully separable states [14, 18, 25]. Since the fully separable set is strictly contained within the biseparable set, this geometric measure constitutes a weaker entanglement criterion compared to other measures that quantify genuine multipartite entanglement [14].

While bipartite entanglement dynamics in open quantum

systems have been fairly well studied [26, 27], studies on evolution of GME in open quantum systems remain scarce. Recent studies on GME in the context of open systems have been either restricted to a few body systems [28–30] or non-interacting models [31–34]. For interacting many-body systems, however, interactions, such as anisotropy in spin models, can counterintuitively enhance robustness against thermal noise. Physically, interactions act as controllable parameters that stabilize the system against decoherence by regulating excitation gaps in the system spectrum, thereby suppressing the thermal fluctuations arising from a broadband bath.

In this context, the anisotropic XXZ spin chain provides a platform where the generalized GHZ and the generalized W states appear naturally in the eigenspectrum. Furthermore, this model can be experimentally realized in solid-state magnets and cold-atom platforms, where the anisotropy parameter can be externally controlled [35, 36].

In this letter, using the Master equation approach integrated with the Bethe ansatz, we analytically demonstrate that the open-system dynamics of multipartite entanglement, associated with these generalized GHZ and W states is controlled by the anisotropy, particularly at low temperatures.

Scenario: Using the Pauli matrices $\vec{\sigma}$ and $\vec{\zeta}$ to represent the spin operators of the system and the bath, respectively, the Hamiltonian of the composite system is written as $H =$

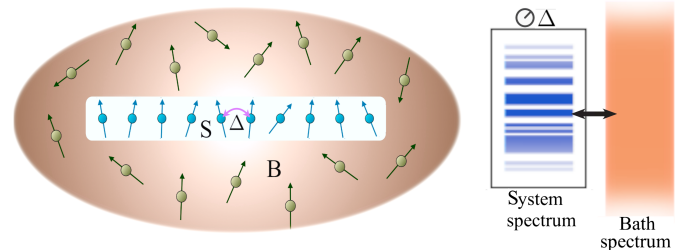


Figure 1. Schematic of an interacting one-dimensional spin chain embedded in a spin bath. The intra-chain anisotropy can be externally tuned to control the multipartite entanglement against broadband thermal fluctuations.

$H_S + H_B + H_{SB}$, where

$$H_S = -\frac{1}{2} \sum_{i=1}^N (\sigma_i^x \sigma_{i+1}^x + \sigma_i^y \sigma_{i+1}^y + \Delta \sigma_i^z \sigma_{i+1}^z),$$

$$H_B = \sum_{k=1}^{N_b} \omega_k \zeta_k^z, \quad H_{SB} = \sum_{i=1}^N \sum_{k=1}^{N_b} g_{ik} (\sigma_i^+ \zeta_k^- + \text{H.c.}). \quad (1)$$

denote the Hamiltonians of the system, the spin-bath, and the system–bath interaction, respectively. The parameter Δ in H_S is the anisotropy parameter, which controls the interaction strength between spins aligned in the same direction. The states $|0\rangle$ ($|1\rangle$) are the eigenstates of the Pauli operator σ^z with eigenvalues $+1$ (-1). A schematic of the system is shown in Fig. 1.

The system exhibits distinct quantum phases depending on the anisotropy: for $\Delta > 1$ and $\Delta < -1$, the ground state exhibits ferromagnetic and antiferromagnetic Néel order respectively with a finite excitation gap; for $-1 < \Delta < 1$, the ground state is in a gapless critical phase.

The bath consists of N_b non-interacting spin- $\frac{1}{2}$ particles, with ω_k denoting the transition frequency of the k th bath spin, distributed isotropically and homogeneously in space [37]. Each bath spin is prepared in a thermal state $\rho_k = p(\beta, \omega_k) |0\rangle\langle 0| + [1 - p(\beta, \omega_k)] |1\rangle\langle 1|$, where the population $p(\beta, \omega_k) = e^{-\beta\omega_k} / [2 \cosh(\beta\omega_k)]$ corresponds to a Gibbs distribution at inverse temperature β . We further assume that the bath frequencies form a broad and dense spectrum in the energy domain, such that it acts as a thermal reservoir. The system-bath coupling g_{ik} is assumed to be weak and bilinear, allowing for slow exchange of excitations between the system and the bath via a flip-flop interaction [4]. We consider the thermodynamic limit in which both the system size N and the bath size N_b tend to infinity, with the ratio $N/N_b (\equiv f)$ kept less than unity.

The Hilbert space of the system decomposes into magnetization sectors labeled by the number of down spins l relative to the fully polarized state $|0\rangle^{\otimes N}$. A basis for the l -magnon subspace is given by the ordered configurations $|\mathbf{x}_l\rangle \equiv |x_1, x_2, \dots, x_l\rangle$, where x_j denotes the lattice position of the j -th down spin. The corresponding eigenstates are $|\Psi_l(\mathbf{q}_l)\rangle = \sum_{\mathbf{x}_l} \psi(\mathbf{q}_l | \mathbf{x}_l) |\mathbf{x}_l\rangle$, where $\psi(\mathbf{q}_l | \mathbf{x}_l)$ is the Bethe wavefunction amplitude and the set $\mathbf{q}_l = (q_1, q_2, \dots, q_l)$ are the Bethe roots or quasi-momenta that are obtained by solving the Bethe ansatz equations [1, 2].

The dynamics of the system in the presence of the bath is described, under weak system-bath coupling, by the second-order time-convolutionless (TCL) master equation. In the interaction picture, the reduced density matrix (RDM) of the system, $\rho_S(t)$, obeys [4]

$$\dot{\rho}_S(t) = - \int_0^t d\tau \Sigma^{(2)}(t, \tau) \rho_S(t), \quad (2a)$$

where the second-order self-energy superoperator is given by

$$\Sigma^{(2)}(t, \tau) = \text{Tr}_B([H_{SB}(t), [H_{SB}(t - \tau), (\cdot) \rho_B]]) . \quad (2b)$$

Here, $H_{SB}(t) = e^{i(H_S + H_B)t} H_{SB} e^{-i(H_S + H_B)t}$ denotes the system-bath coupling Hamiltonian in the interaction picture with respect to the free Hamiltonians H_S and H_B of the system and the bath, respectively. Assuming a system invariant under lattice translations, and coupled to an isotropic and homogeneous environment via translationally invariant couplings (i.e., $g_{ik} = g(k)$) ensures the conservation of total momentum in the interaction processes governing the open-system dynamics.

Generalized GHZ state.— We start by looking at the evolution and the decoherence of the generalized GHZ state in the presence of the bath. The generalized GHZ state $(|0\rangle^{\otimes N} + |1\rangle^{\otimes N}) / \sqrt{2}$ is an equal coherent superposition of the zero-magnon and N -magnon Bethe eigenstates. The time-dependent state of the system initialized with the generalized GHZ state reads in the Bethe basis $\{|\Psi_0\rangle, |\Psi_1(q=0)\rangle, |\Psi_{N-1}(q=0)\rangle, |\Psi_N\rangle\}$ as (see S.I. I)

$$\rho(t) = \begin{pmatrix} \frac{u}{2} & 0 & 0 & v \\ 0 & \frac{1-u}{2} & 0 & 0 \\ 0 & 0 & \frac{1-u}{2} & 0 \\ v & 0 & 0 & \frac{u}{2} \end{pmatrix}, \quad (3a)$$

with the time-dependent population (diagonal) and coherence (off-diagonal) terms obtained by solving the ME in Eq. (31a)

$$u(t) = 1 - \frac{e^{-\beta(1-\Delta)}}{\cosh \beta(1-\Delta)} (1 - e^{-\pi t \gamma f n}),$$

$$v(t) = \frac{1}{2} e^{-\pi t \gamma f n} \frac{e^{-\beta(1-\Delta)}}{2 \cosh \beta(1-\Delta)}, \quad (3b)$$

Here n denotes the density of states for the bath spins, and γ is an effective decay parameter that depends on several microscopic features of the composite system, including the spatial distribution of bath spins and the dimensionality of the surrounding environment (see S.I. II for the explicit form of γ). The temperature and the anisotropy together dictate the dissipation rates through the Gibbs factor. Population transfer from the state $|\Psi_0\rangle$ to $|\Psi_1(q=0)\rangle$ (or from $|\Psi_N\rangle$ to $|\Psi_{N-1}(q=0)\rangle$) occurs on a time scale inversely proportional to the product $\gamma f n$, while the coherence decays on a time scale inversely proportional to $\gamma f n$ multiplied by a temperature-dependent Gibbs factor.

Both the population and coherence terms in Eq. (3b) exhibit a non-analytic behavior at $\Delta = 1$ in the low-temperature limit. This non-analyticity originates from the exponential factor $\exp\{-\beta(1-\Delta)\}$, as its asymptotic behavior changes discontinuously as $\Delta \rightarrow 1^\pm$. This exponential factor originates from the transition rate connecting the zero-magnon and one-magnon sectors. As a result, the dissipative dynamics differs qualitatively between the regimes $\Delta < 1$ and $\Delta > 1$: in the low-temperature limit, both population exchange and coherence decay are strongly enhanced for $\Delta > 1$, whereas the state remains comparatively robust for $\Delta < 1$. This non-

analyticity in the dissipative rates propagates to sharp features in time-dependent entanglement measures across the critical point $\Delta = 1$, as we shall discuss below.

To characterize the GME of the state in Eq. 3a, we first look at the *geometric measure* of GME. It is defined for a generic mixed state of the form $\rho = \sum_i p_i |\psi_i\rangle\langle\psi_i|$ as the convex-roof minimization of the GME of its pure state components [10, 13, 18, 25] as

$$E_G(\rho) \equiv \min_{\{p_i, |\psi_i\rangle\}} \sum_i p_i E_G(|\psi_i\rangle), \quad (4)$$

where the pure state GME measure $E_G(|\psi\rangle) \equiv 1 - \max_{|\Phi\rangle} |\langle\Phi|\psi\rangle|^2$ is computed by maximization over all pure biseparable states Φ . For a state with incoherent mixture of orthogonal components supported on different excitation-number sectors of the form Eq. (3a), a closed form expression for the upper-bound can be evaluated directly from computing the GME of its components as $E_G(\rho) \leq \frac{u}{2} E_G(\rho_{GHZ}) + (1-u) E_G(|\Psi_1(q=0)\rangle)$. The first term on the right hand side of the inequality appears from the zero-magnon and N -magnon sector; whereas the second term from the one-magnon and $(N-1)$ -magnon sector. Now, it can be shown that the geometric GME of the generalized W state is non-extensive, i.e., it scales as N^{-1} with the system size N (see S.I. IVC). Therefore, in the thermodynamic limit, the contribution from the single-magnon and $(N-1)$ -magnon sectors vanishes, and the expression becomes exact [10, 11, 43, 45](see S.I. IVA):

$$E_G(\rho) = \frac{u}{2} \left(1 - \sqrt{1 - \frac{4v^2}{u^2}} \right), \quad (5)$$

with u and v given in Eq. (3b).

Although the geometric measure of GME provides a definition of nonclassical correlations without reference to any specific task [10, 46], the distillation fraction is an operational and protocol-dependent notion, quantifying how much useful GME can be extracted via LOCC [6, 7, 22, 47, 48, 50, 51]. As a result, a nonzero geometric measure does not guarantee a finite distillation, particularly in the thermodynamic limit. We adopt Murao et al.'s protocol since it directly distills GHZ-type multipartite entanglement under LOCC and provides a simple computable distillation rate, and is straightforward to generalize for large many-body systems [6]. The protocol provides an operational method for extracting N -qubit GHZ states from many imperfect copies shared among spatially separated parties. Because GME cannot be concentrated or distilled using only bipartite operations, the protocol relies on LOCC among all parties. Through successive rounds of coordinated local measurements, parity checks, and conditional post-selection, the input state is filtered toward the GHZ subspace. The asymptotic lower bound of the distillable GHZ entanglement of the purification scheme in the thermodynamic limit ($N \rightarrow \infty$) is given by (see S.I. III),

$$\mathcal{E}_D^{\text{GHZ}} = \max_{r \geq 0} \left[u^{(2^{r+1}-2)} (1 - h(P_0^r, P_1^r)) \right], \quad (6)$$

with $h(P_0^r, P_1^r)$ denoting the Shannon entropy of the marginal phase-error distribution of the state obtained from r th iteration of the protocol.

The dynamics of GME across the anisotropy landscape exhibits a clear distinction between the regimes $\Delta < 1$ and $\Delta > 1$ in the presence of a thermal bath: the region $\Delta < 1$ is favorable for retaining GHZ-type correlations with time, whereas the region $\Delta > 1$ leads to the loss of GHZ correlations and instead generates single-excitation states with Dicke-type correlations (Fig. 2(a) and (c)). For anisotropy $\Delta < 1$, both the distillation fraction and the geometric GME decay to zero beyond a threshold temperature in asymptotic time, indicating a temperature threshold of preserving the GHZ state (Fig. 2(b) and (d)). In contrast, for anisotropy $\Delta > 1$, both the distillation fraction and the GME decay to zero rapidly at any non zero temperature, indicating that this regime lacks the multipartite coherence structure necessary for distillation of GHZ states (Fig. 2(d)). However, physically, the non-analyticity of GME at $\Delta = 1$ in the low temperature limit for a thermal bath owes to the change in the low-energy spectral properties of the underlying XXZ model. The crossover point, interestingly, marks the Heisenberg isotropic point which separates the gapless and the gapped regimes [1].

For the regime $\Delta < 1$, once the temperature exceeds a critical value, the onset of thermal fluctuations in the system leads to an inevitable loss of GHZ correlations due to statistical mixing of eigenstates. The loss of GME can be characterized in terms of an effective incoherent admixture induced by the bath. In the long-time limit, the dynamics generates a temperature-dependent mixing parameter $p(\beta_c, 1 - \Delta) = x$, set by the system energy scale $(1 - \Delta)$, assuming detectable GME persists only as long as this admixture remains below a threshold x . Here we estimate the threshold value to be $x \approx 0.007$ for both GME and distillation fraction. A characteristic temperature scale therefore becomes $\beta_c^{-1} \sim 2(1 - \Delta) \ln[(1 - x)/x]$. For some fixed x , this implies a logarithmic dependence of the GME retention temperature on anisotropy, when plotted in semi-logarithmic axes, as evident from Fig. 2(b) and (d). The temperature-anisotropy dependence of GME in our case exhibits a wedge-like structure reminiscent of the quantum-criticality observed near quantum phase transitions [53]

Generalized W state.— The generalized W state $\sum_{i=1}^N |0 \cdots 1_i \cdots 0\rangle / \sqrt{N}$ represents a distinct class of genuinely multipartite entangled state that is inequivalent to the GHZ class under LOCC; as it retains bipartite entanglement in all reduced subsystems [54]. In our setup, this state corresponds to a one-magnon Bethe eigenstate with zero total momentum [2, 55]. The formal solution of the master equation initialized with the generalized W state involves contributions from the zero-magnon eigenstate, and two-magnon eigenstates, including both scattering and bound-state configurations.

In the thermodynamic limit, the two-magnon sector forms a continuum of states: the scattering sector, parametrized by a relative quasi-momentum $q \in (0, \pi)$, describes delocalized magnons, while the bound sector corresponds to localized spin-pair excitations [2, 3] (see S.I. I). As shown in Appendix B,

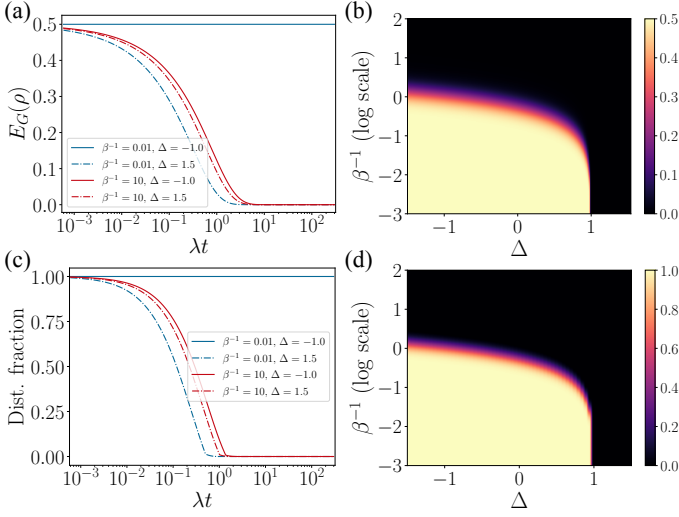


Figure 2. *Dynamics of the generalized GHZ state.* (a,b) geometric genuine multipartite entanglement: (a) as a function of scaled time (λt) for different temperatures and anisotropies, and (b) as a function of temperature and anisotropy at long times ($\lambda t = 100$). (c,d) Lower bound of the distillation fraction: (c) as a function of scaled time (λt) for different temperatures and anisotropies, and (d) as a function of temperature and anisotropy at long times ($\lambda t = 100$). The plots are generated using $N/N_b \equiv f = 0.01$, effective decay rate $\gamma = 1$, and average bath spectral density $n = 10$.

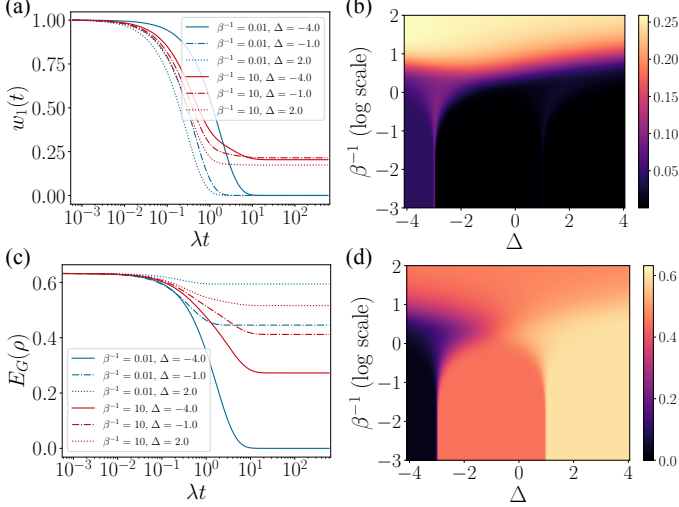


Figure 3. *Dynamics of the generalized W state.* (a,b) Fraction of the generalized W state in the classical mixture: (a) as a function of scaled time (λt) for different temperatures and anisotropies, and (b) as a function of temperature and anisotropy at long times ($\lambda t = 100$). (c,d) Upper bound of the geometric collective multipartite entanglement: (c) as a function of scaled time (λt) for different temperatures and anisotropies, and (d) as a function of temperature and anisotropy at long times ($\lambda t = 100$). The plots are generated using $N/N_b \equiv f = 0.01$, effective decay rate $\gamma = 1$, and average bath spectral density $n = 10$.

however, only the scattering states with quasi-momenta $q \rightarrow 0^+$ (translation-even states) and $q \rightarrow \pi^-$ (translation-odd states) contribute to the dynamics in the thermodynamic limit. The corresponding transition amplitudes scale as N/N_b , whereas the same associated with finite- q scattering states and bound states scale as $1/(NN_b)$ and $1/N_b$, respectively, and are therefore suppressed in the thermodynamic limit (see S.I. II). As a consequence, a closed-form time-dependent solution in the thermodynamic limit in the Bethe basis $\{|\Psi_0\rangle, |\Psi_1(q=0)\rangle, |\Psi_2(q=0^+)\rangle, |\Psi_2(q=\pi^-)\rangle\}$ reads

$$\rho(t) = \begin{pmatrix} w_0 & 0 & 0 & 0 \\ 0 & w_1 & 0 & 0 \\ 0 & 0 & w_2(0^+) & 0 \\ 0 & 0 & 0 & w_2(\pi^-) \end{pmatrix}. \quad (7)$$

The time-dependent population terms $\mathbf{w} \equiv (w_0, w_1, w_2(0^+), w_2(\pi^-))$ are obtained solving the ME in Eq. (31a) as

$$\mathbf{w}(t) = \exp\{\mathcal{M}(\beta, \Delta)t\}\mathbf{w}(0), \quad (8)$$

where the matrix $\mathcal{M}(\beta, \Delta)$ has the form of Markov generator [57, 58] (see S.I. IIC for the expression of $\mathbf{w}(t)$). The matrix $\mathcal{M}(\beta, \Delta)$ consists of several transition amplitudes of the dissipative rates between the energy levels. However, at low temperature, one can infer from the structure of the matrix $\mathcal{M}(\beta, \Delta)$ that only certain transitions are allowed. If the system is initialized in the generalized W state, then in the anisotropy regime $\Delta < -3$ only the transition $|\Psi_1(q=0)\rangle \rightarrow |\Psi_0\rangle$ is favored. In the regime $-3 < \Delta < 1$, the transitions $|\Psi_1(q=0)\rangle \rightarrow |\Psi_0\rangle$ and $|\Psi_1(q=0)\rangle \rightarrow |\Psi_2(q=\pi^-)\rangle$ are favored. For $\Delta > 1$, the allowed transitions are $|\Psi_1(q=0)\rangle \rightarrow |\Psi_0\rangle$, $|\Psi_1(q=0)\rangle \rightarrow |\Psi_2(q=0^+)\rangle$, and $|\Psi_1(q=0)\rangle \rightarrow |\Psi_2(q=\pi^-)\rangle$.

As a consequence, the fraction of the W state in the classical ensemble decays monotonically with time, irrespective of the anisotropy and temperature (Fig. 3(a)). However, at asymptotically long times, this fraction is higher (≈ 0.25) above the threshold temperature β_c^{-1} than at low temperature, due to thermal mixing of eigenstates. The point $\Delta = -3$ marks a boundary: below it, the dynamics predominantly generates unentangled states, whereas above it, two-magnon Dicke-type correlated states emerge (Fig. 3(b)).

The entanglement of the state in (7) is bounded by the convex roof criterion: $E_G(\rho) \leq w_1 E_G(|\Psi_1(q=0)\rangle) + w_2(0^+) E_G(|\Psi_2(q=0^+)\rangle) + w_2(\pi^-) E_G(|\Psi_2(q=\pi^-)\rangle)$. The main challenge in computing the geometric GME for this state in the thermodynamic limit is because of the non-extensivity of the measure. We show that for the one magnon W state and the two-magnon states $|\Psi_2(q=0^+)\rangle, |\Psi_2(q=\pi^-)\rangle$, the geometric GME scale as $\mathcal{O}(N^{-1})$ respectively with system size (see S.I. IVD), implying that this measure is unsuitable in the thermodynamic limit. But for completeness and to better characterize the multipartite correlations, we compute the geometric measure of CME, a multipartite entan-

glement measure obtained by maximizing over fully separable multipartite states in Eq. (4) [14]. In the thermodynamic limit, $E_G(|\Psi_1(q=0)\rangle) = (1 - 1/e)$, $E_G(|\Psi_2(q=0^+)\rangle) = E_G(|\Psi_2(q=\pi^-)\rangle) = (1 - 3/e^2)$. Therefore, upper bound of the CME of the state in (7) becomes (see S.I. IVD)

$$E_G(\rho) \leq \left(1 - \frac{1}{e}\right) w_1 + \left(1 - \frac{3}{e^2}\right) (w_2(0^+) + w_2(\pi^-)). \quad (9)$$

The upper bound of CME shows strongly anisotropy-dependence, particularly in the low temperature regime: (a) the system loses CME to zero due to the presence of unentangled states. (b) For anisotropy in the range $-3 < \Delta < 1$, state becomes an incoherent mixture of unentangled and a genuinely entangled state: $\{|\Psi_0\rangle, |\Psi_2(q=\pi^-)\rangle\}$; thereby preserving entanglement in the system, but in the form of two-excitation translation-odd states. (c) For any anisotropy $\Delta \geq 1$, the state becomes an incoherent mixture of the zero magnon, two magnon states with momenta $q = 0^+$ and $q = \pi^-$, thereby retaining highest value CME in the system. Figure 3(c) and (d) show this nontrivial crossovers at $\Delta = -3$ and $\Delta = 1$, separating a low-entanglement to an intermediate entanglement, and an intermediate entanglement to a high entanglement region. However, beyond the critical temperature, transitions between all the eigenstates have finite probabilities, implying the system has a nonvanishing value of CME regardless of the anisotropy, but the one-excitation Dicke type entanglement is lost.

Although entanglement remains finite at finite temperature as the dynamics explores multiple excitation sectors, the W type entanglement is lost in the system. This makes distillation of large N generalized W -state challenging which is evident from any distillation based measure of GME. For a mixed state of the form Eq. (7), no LOCC distillation protocol is known that yields a nonzero asymptotic distillation fraction of generalized W states in the thermodynamic limit [9, 59]. For finite system sizes, local projective measurements on a symmetric two-excitation Dicke state, can probabilistically collapse the remaining qubits into a W -type entangled state [60, 61]. However, no general LOCC protocol is known that converts a two-excitation Dicke state into an N -qubit W state with finite distillation fraction for arbitrary N , particularly in the large- N limit.

Discussions and Conclusions. Our model considers a broad class of experimentally relevant situations in which an interacting one-dimensional quantum magnet is embedded in an infinite spin bath environment, where anisotropy is tunable via chemical doping or applied strain [62–67]. Trapped-ion platforms can provide controllable quantum simulators of XXZ chains with tunable anisotropy controlled by lattice depths [35, 68, 69]. In a realistic quasi-one-dimensional Cu-based spin chain with exchange energy $J \sim 5$ meV ($J/k_B \approx 58$ K), the survival of multipartite entanglement is governed by the Gibbs weight of the transition energy. Imposing a threshold population $x \approx 0.007$ yields an estimate for the critical temperature $T_c \approx 12$ K, well within experimentally accessible

low-temperature regimes.

To conclude, we analytically show that the anisotropy present in the intra-system interactions plays a decisive role in the survival of GME and CME, particularly in the low temperature. We show, that thermal noise is not generically destructive for multipartite correlations but makes difficult for its distillation. From the perspective of modern quantum computing, our results demonstrate that Hamiltonian engineering, particularly, by tuning interaction anisotropy, one can stabilize entanglement even against thermal noise. Our approach paves a way to design more fine-tuned control of intra-system interaction against colored noise, noise arising from qubit-boson interactions. Through this control it is possible to engineer entanglement-resilient subspaces without suppressing system-environment coupling, which is rather technologically challenging.

ACKNOWLEDGEMENT

The authors are grateful to Sibasish Ghosh, Diptiman Sen, and V. Subrahmanyam for fruitful discussions. This work was supported by the Swiss National Science Foundation under Division II (Grant No. 200020-219400).

* samudra.sur@unige.ch

† author for correspondence; saikats@imsc.res.in

- [1] H. D. Zeh, “On the interpretation of measurement in quantum theory,” *Foundations of Physics* **1**, 69–76 (1970).
- [2] David P. DiVincenzo, “The physical implementation of quantum computation,” *Fortschritte der Physik* **48**, 771–783 (2000).
- [3] Wojciech Hubert Zurek, “Decoherence, einselection, and the quantum origins of the classical,” *Rev. Mod. Phys.* **75**, 715–775 (2003).
- [4] Mark Hillery, Vladimír Bužek, and André Berthiaume, “Quantum secret sharing,” *Phys. Rev. A* **59**, 1829–1834 (1999).
- [5] Richard Cleve, Daniel Gottesman, and Hoi-Kwong Lo, “How to share a quantum secret,” *Phys. Rev. Lett.* **83**, 648–651 (1999).
- [6] Otfried Gühne and Geza Toth, “Entanglement detection,” *Physics Reports* **474**, 1–75 (2009).
- [7] Ryszard Horodecki, Paweł Horodecki, Michał Horodecki, and Karol Horodecki, “Quantum entanglement,” *Rev. Mod. Phys.* **81**, 865–942 (2009).
- [8] Michael Epping, Hermann Kampermann, Chiara Macchiavello, and Dagmar Bruß, “Multi-partite entanglement can speed up quantum key distribution in networks,” *New Journal of Physics* **19**, 093012 (2017).
- [9] Nicolas Brunner, Daniel Cavalcanti, Stefano Pironio, Valerio Scarani, and Stephanie Wehner, “Bell nonlocality,” *Rev. Mod. Phys.* **86**, 419–478 (2014).
- [10] Anders Karlsson and Mohamed Bourennane, “Quantum teleportation using three-particle entanglement,” *Phys. Rev. A* **58**, 4394–4400 (1998).
- [11] Ping-Xing Chen, Shi-Yao Zhu, and Guang-Can Guo, “General form of genuine multipartite entanglement quantum channels for teleportation,” *Phys. Rev. A* **74**, 032324 (2006).

- [12] Géza Tóth, “Multipartite entanglement and high-precision metrology,” *Phys. Rev. A* **85**, 022322 (2012).
- [13] Robert Raussendorf and Hans J. Briegel, “A one-way quantum computer,” *Phys. Rev. Lett.* **86**, 5188–5191 (2001).
- [14] H. J. Briegel, D. E. Browne, W. Dür, R. Raussendorf, and M. Van den Nest, “Measurement-based quantum computation,” *Nature Physics* **5**, 19–26 (2009).
- [15] Daniel Gottesman, “Stabilizer codes and quantum error correction,” (1997), [arXiv:quant-ph/9705052](https://arxiv.org/abs/quant-ph/9705052) [quant-ph].
- [16] A. Yu. Kitaev, “Quantum computations: algorithms and error correction,” in *Proceedings of the International Congress of Mathematicians*, Vol. 1 (1997) pp. 661–672.
- [9] W. Dür, G. Vidal, and J. I. Cirac, “Three qubits can be entangled in two inequivalent ways,” *Phys. Rev. A* **62**, 062314 (2000).
- [18] Abner Shimony, “Degree of entanglement,” *Annals of the New York Academy of Sciences* **755**, 675–679 (1995).
- [19] A. Acín, D. Bruß, M. Lewenstein, and A. Sanpera, “Classification of mixed three-qubit states,” *Phys. Rev. Lett.* **87**, 040401 (2001).
- [20] Michael Seevinck and Jos Uffink, “Partial separability and entanglement criteria for multiqubit quantum states,” *Phys. Rev. A* **78**, 032101 (2008).
- [21] J. Eisert, M. Cramer, and M. B. Plenio, “Colloquium: Area laws for the entanglement entropy,” *Rev. Mod. Phys.* **82**, 277–306 (2010).
- [22] W. Dür, J. I. Cirac, and R. Tarrach, “Separability and distillability of multiparticle quantum systems,” *Phys. Rev. Lett.* **83**, 3562–3565 (1999).
- [23] Michał Horodecki, Paweł Horodecki, and Ryszard Horodecki, “Limits for entanglement measures,” *Phys. Rev. Lett.* **84**, 2014–2017 (2000).
- [14] Tzu-Chieh Wei and Simone Severini, “Matrix permanent and quantum entanglement of permutation invariant states,” *Journal of Mathematical Physics* **51**, 092203 (2010).
- [25] H Barnum and N Linden, “Monotones and invariants for multiparticle quantum states,” *Journal of Physics A: Mathematical and General* **34**, 6787 (2001).
- [26] Ting Yu and J. H. Eberly, “Finite-time disentanglement via spontaneous emission,” *Phys. Rev. Lett.* **93**, 140404 (2004).
- [27] Jens Clausen, Guy Bentsky, and Gershon Kurizki, “Task-optimized control of open quantum systems,” *Phys. Rev. A* **85**, 052105 (2012).
- [28] ZhiHao Ma, ZhiHua Chen, and Felipe Fernandes Fanchini, “Multipartite quantum correlations in open quantum systems,” *New Journal of Physics* **15**, 043023 (2013).
- [29] Ankit Vaishy, Subhadip Mitra, and Samyadeb Bhattacharya, “Detecting genuine multipartite entanglement in three-qubit systems with eternal non-markovianity,” *Journal of Physics A: Mathematical and Theoretical* **55**, 225305 (2022).
- [30] Sovik Roy, Md. Manirul Ali, Abhijit Mandal, and Chandrashekar Radhakrishnan, “Dephasing-induced distribution of entanglement in tripartite quantum systems,” *Modern Physics Letters A* **40** (2025), 10.1142/s0217732325500828.
- [31] Qing-Yang Qiu, Zhi-Guang Lu, Qiongyi He, Ying Wu, and Xin-You Lü, “Genuine multipartite entanglement induced by a thermal acoustic reservoir,” *Phys. Rev. B* **110**, L220301 (2024).
- [32] André R. R. Carvalho, Florian Mintert, and Andreas Buchleitner, “Decoherence and multipartite entanglement,” *Phys. Rev. Lett.* **93**, 230501 (2004).
- [33] S. M. Hashemi Rafsanjani, M. Huber, C. J. Broadbent, and J. H. Eberly, “Genuinely multipartite concurrence of n -qubit x matrices,” *Phys. Rev. A* **86**, 062303 (2012).
- [34] Abhinash Kumar Roy, Sourabh Magare, Varun Srivastava, and Prasanta K. Panigrahi, “Exact time evolution of genuine multipartite correlations for n -qubit systems in a common thermal reservoir,” *Quantum Reports* **4**, 22–35 (2022).
- [35] A. Friedenauer, H. Schmitz, J. T. Glueckert, D. Porras, and T. Schaetz, “Simulating a quantum magnet with trapped ions,” *Nature Physics* **4**, 757–761 (2008).
- [36] R. Islam, E. E. Edwards, K. Kim, S. Korenblit, C. Noh, H. Carmichael, G.-D. Lin, L.-M. Duan, C.-C. Joseph Wang, J. K. Freericks, and C. Monroe, “Onset of a quantum phase transition with a trapped ion quantum simulator,” *Nature Communications* **2**, 377 (2011).
- [37] D. D. Bhaktavatsala Rao and Gershon Kurizki, “From zeno to anti-zeno regime: Decoherence-control dependence on the quantum statistics of the bath,” *Phys. Rev. A* **83**, 032105 (2011).
- [4] H. P. Breuer and F. Petruccione, *The theory of open quantum systems* (Oxford University Press, Great Clarendon Street, 2002).
- [1] H. Bethe, “Zur theorie der metalle,” *Zeitschrift für Physik* **71**, 205–226 (1931).
- [2] Yu. A. Izyumov and Yu. N. Skryabin, *Statistical Mechanics of Magnetically Ordered Systems* (Springer-Verlag, Heidelberg, 1988).
- [13] Tamoghna Das, Sudipto Singha Roy, Shrobona Bagchi, Avijit Misra, Aditi Sen(De), and Ujjwal Sen, “Generalized geometric measure of entanglement for multiparty mixed states,” *Phys. Rev. A* **94**, 022336 (2016).
- [10] Tzu-Chieh Wei and Paul M. Goldbart, “Geometric measure of entanglement and applications to bipartite and multipartite quantum states,” *Phys. Rev. A* **68**, 042307 (2003).
- [43] John A. Smolin, Frank Verstraete, and Andreas Winter, “Entanglement of assistance and multipartite state distillation,” *Phys. Rev. A* **72**, 052317 (2005).
- [11] Robert Hübener, Matthias Kleinmann, Tzu-Chieh Wei, Carlos González-Guillén, and Otfried Gühne, “Geometric measure of entanglement for symmetric states,” *Phys. Rev. A* **80**, 032324 (2009).
- [45] Christopher Eltschka and Jens Siewert, “Quantifying entanglement resources,” *Journal of Physics A: Mathematical and Theoretical* **47**, 424005 (2014).
- [46] Marcus Huber, Martí Perarnau-Llobet, and Julio I. de Vicente, “Entropy vector formalism and the structure of multidimensional entanglement in multipartite systems,” *Phys. Rev. A* **88**, 042328 (2013).
- [47] Charles H. Bennett, Herbert J. Bernstein, Sandu Popescu, and Benjamin Schumacher, “Concentrating partial entanglement by local operations,” *Phys. Rev. A* **53**, 2046–2052 (1996).
- [48] Charles H. Bennett, Gilles Brassard, Sandu Popescu, Benjamin Schumacher, John A. Smolin, and William K. Wootters, “Purification of noisy entanglement and faithful teleportation via noisy channels,” *Phys. Rev. Lett.* **76**, 722–725 (1996).
- [6] M. Murao, M. B. Plenio, S. Popescu, V. Vedral, and P. L. Knight, “Multiparticle entanglement purification protocols,” *Phys. Rev. A* **57**, R4075–R4078 (1998).
- [50] M. Murao, D. Jonathan, M. B. Plenio, and V. Vedral, “Quantum telecloning and multiparticle entanglement,” *Phys. Rev. A* **59**, 156–161 (1999).
- [51] J Clausen, L Knoll, and D-G Welsch, “Entanglement purification of multi-mode quantum states,” *Journal of Optics B: Quantum and Semiclassical Optics* **5**, S561 (2003).
- [7] W Dur and H J Briegel, “Entanglement purification and quantum error correction,” *Reports on Progress in Physics* **70**, 1381 (2007).
- [53] Subir Sachdev, *Quantum Phase Transitions* (Cambridge University Press, 1999).
- [54] W. Dür, G. Vidal, and J. I. Cirac, “Three qubits can be entangled in two inequivalent ways,” *Phys. Rev. A* **62**, 062314 (2000).

- [55] Michel Gaudin, *The Bethe Wavefunction*, edited by Jean-Sébastien Caux (Cambridge University Press, 2014).
- [3] Chanchal K. Majumdar, G. Mukhopadhyay, and A. K. Rajagopal, “A simple derivation of the three magnon bound state equation,” *Pramana* **1**, 135–146 (1973).
- [57] Vittorio Gorini, Andrzej Kossakowski, and E. C. G. Sudarshan, “Completely positive dynamical semigroups of n -level systems,” *Journal of Mathematical Physics* **17**, 821–825 (1976).
- [58] Herbert Spohn, “Kinetic equations from hamiltonian dynamics: Markovian limits,” *Rev. Mod. Phys.* **52**, 569–615 (1980).
- [59] David Sauerwein, Nolan R. Wallach, Gilad Gour, and Barbara Kraus, “Transformations among pure multipartite entangled states via local operations are almost never possible,” *Phys. Rev. X* **8**, 031020 (2018).
- [60] A. Chiuri, C. Greganti, M. Paternostro, G. Vallone, and P. Mataloni, “Experimental quantum networking protocols via four-qubit hyperentangled dicke states,” *Phys. Rev. Lett.* **109**, 173604 (2012).
- [61] Witłef Wieczorek, Roland Krischek, Nikolai Kiesel, Patrick Michelberger, Géza Tóth, and Harald Weinfurter, “Experimental entanglement of a six-photon symmetric dicke state,” *Phys. Rev. Lett.* **103**, 020504 (2009).
- [62] Masashi Hase, Ichiro Terasaki, and Kunimitsu Uchinokura, “Observation of the spin-peierls transition in linear Cu^{2+} (spin-1/2) chains in an inorganic compound CuGeO_3 ,” *Phys. Rev. Lett.* **70**, 3651–3654 (1993).
- [63] M. Takigawa, N. Motoyama, H. Eisaki, and S. Uchida, “Dynamics in the $S = 1/2$ one-dimensional antiferromagnet Sr_2CuO_3 via ^{63}Cu nmr,” *Phys. Rev. Lett.* **76**, 4612–4615 (1996).
- [64] R. Toskovic, R. van den Berg, A. Spinelli, I. S. Eliens, B. van den Toorn, B. Bryant, J.-S. Caux, and A. F. Otte, “Atomic spin-chain realization of a model for quantum criticality,” *Nature Physics* **12**, 656–660 (2016).
- [65] Dalila Bounoua, Romuald Saint-Martin, Sylvain Petit, Patrick Berthet, Françoise Damay, Yvan Sidis, Frédéric Bourdarot, and Loreynne Pinsard-Gaudart, “Impurity-induced spin pseudogap in SrCuO_2 doped with mg, zn, or la,” *Phys. Rev. B* **95**, 224429 (2017).
- [66] W. M. Witzel and S. Das Sarma, “Quantum theory for electron spin decoherence induced by nuclear spin dynamics in semiconductor quantum computer architectures: Spectral diffusion of localized electron spins in the nuclear solid-state environment,” *Phys. Rev. B* **74**, 035322 (2006).
- [67] N V Prokof'ev and P C E Stamp, “Theory of the spin bath,” *Reports on Progress in Physics* **63**, 669 (2000).
- [68] Immanuel Bloch, Jean Dalibard, and Wilhelm Zwerger, “Many-body physics with ultracold gases,” *Rev. Mod. Phys.* **80**, 885–964 (2008).
- [69] K. Kim, M.-S. Chang, S. Korenblit, R. Islam, E. E. Edwards, J. K. Freericks, G.-D. Lin, L.-M. Duan, and C. Monroe, “Quantum simulation of frustrated ising spins with trapped ions,” *Nature* **465**, 590–593 (2010).

BETHE ANSTAZ SOLUTION FOR THE ANISOTROPIC XXZ MODEL

The Bethe ansatz wavefunction in the l -magnon sector is expressed as a superposition of plane waves [1, 2]

$$|\Psi_l(\mathbf{q})\rangle = \sum_{x_1, \dots, x_l} \psi(\mathbf{q}|\mathbf{x}) |\mathbf{x}\rangle, \quad (10)$$

with

$$\psi(\mathbf{q}|\mathbf{x}) = \sum_{\Pi} A_{\Pi} \exp\left(i \sum_{j=1}^l q_{\Pi_j} x_j\right), \quad (11)$$

where q_1, \dots, q_l are real or complex quasi-momenta of the magnons, Π denotes permutations of these quasi-momenta, and the amplitudes A_{Π} are fixed by two-body scattering phases.

The Bethe roots are obtained by solving the coupled set of l Bethe equations

$$Nq_j = 2\pi I_j - \sum_{\substack{k=1 \\ k \neq j}}^l \Theta(q_j, q_k),$$

$$\Theta(q_j, q_k) = 2 \cot^{-1} \left(\frac{\Delta \sin \frac{q_j - q_k}{2}}{\cos \frac{q_j + q_k}{2} - \Delta \cos \frac{q_j - q_k}{2}} \right), \quad (12)$$

where $\Theta(q_j, q_k)$ is the two-body scattering phase related to the S-matrix by $\mathcal{S}(q_j, q_k) = \exp[i\Theta(q_j, q_k)]$, and $I_j \in \{0, 1, \dots, N-1\}$ are Bethe quantum numbers. The corresponding energy eigenvalues are

$$\epsilon_l = -\frac{N\Delta}{2} + 2 \sum_{j=1}^l (\Delta - \cos q_j). \quad (13)$$

In this article, we consider only net momentum zero sector, i.e., $\sum_i q_i = 0$. The Bethe eigenvalues corresponding to the zero

net-momentum are represented in Fig. 4.

One-magnon states

Starting from the fully polarized ferromagnetic vacuum, a one-magnon excitation is created by flipping a single spin. The one-magnon eigenstates are labeled by the momentum p and have the wavefunction

$$\psi_q(x) = \frac{1}{\sqrt{N}} e^{iqx}, \quad q = \frac{2\pi I_1}{N}, \quad (14)$$

for a periodic chain, where $I_1 = 0, 1, \dots, N-1$. The corresponding energy dispersion is

$$\epsilon_1(q) = -\frac{N\Delta}{2} + 2(\Delta - \cos q). \quad (15)$$

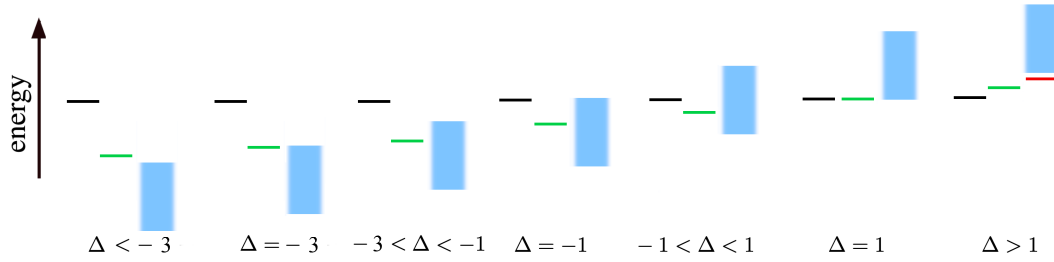


Figure 4. Zero-net-momentum energy eigenvalues of the XXZ model in the thermodynamic limit $N \rightarrow \infty$, corresponding to the zero-magnon sector, the one-magnon sector, and the two-magnon scattering and bound-state sectors. These eigenvalues are represented by black, green, blue, and red lines, respectively.

Two-magnon scattering states

For zero total momentum, $q_1 + q_2 = 0$, we set $q_1 = q$ and $q_2 = -q$. In the thermodynamic limit $N \rightarrow \infty$, the energy eigenvalues are parametrized by a single continuous quantum number $q \in [0, \pi]$ as

$$\epsilon_2(q) = -\frac{N\Delta}{2} + 4(\Delta - \cos q). \quad (16)$$

For $x_2 > x_1$, the corresponding scattering eigenstates take the form

$$\psi_q(x_1, x_2) = A_q \left(e^{-iq(x_2-x_1)} + S(q, -q) e^{iq(x_2-x_1)} \right), \quad q \in (0, \pi), \quad (17)$$

where $S(q, -q) = \exp[i\Theta(q, -q)]$ is the two-magnon scattering matrix.

The normalization factor in Eq. (17) is given by

$$\begin{aligned} A_q^{-2} &= \sum_{x_1=1}^N \sum_{x_2=x_1+1}^{x_1+N-1} |\psi_q(x_1, x_2)|^2 \\ &= N(N-1) + S(q, -q) \mathcal{I}_1(q, N) + S^*(q, -q) \mathcal{I}_2(q, N), \end{aligned} \quad (18)$$

where

$$\begin{aligned}\mathcal{I}_1(q, N) &= \sum_{x_1=1}^N \sum_{x_2=x_1+1}^{x_1+N-1} e^{2iq(x_2-x_1)} = Ne^{2iq} \frac{1 - e^{2iq(N-1)}}{1 - e^{2iq}}, \\ \mathcal{I}_2(q, N) &= \sum_{x_1=1}^N \sum_{x_2=x_1+1}^{x_1+N-1} e^{-2iq(x_2-x_1)} = Ne^{-2iq} \frac{1 - e^{-2iq(N-1)}}{1 - e^{-2iq}},\end{aligned}\quad (19)$$

both of which scale as $\mathcal{O}(N)$, while the leading term scales as $\mathcal{O}(N^2)$.

In the limits $q \rightarrow 0^+$ and $q \rightarrow \pi^-$, the wavefunction in Eq. (17) must be expanded to linear order in q . This yields

$$\begin{aligned}\psi_{q=0^+}(x_1, x_2) &= -2iA_q q (x_2 - x_1), \\ \psi_{q=\pi^-}(x_1, x_2) &= -2iA_q q (-1)^{x_2-x_1} (x_2 - x_1).\end{aligned}\quad (20)$$

The corresponding normalization factors are

$$A_q|_{q \rightarrow 0^+} = A_q|_{q \rightarrow \pi^-} = \frac{1}{2qN\sqrt{\frac{(N-1)(2N-1)}{6}}}.\quad (21)$$

The normalized wavefunctions in these limits therefore become

$$\psi_q(x_1, x_2)|_{q=0^+} = \frac{-i\sqrt{3}}{N^2}(x_2 - x_1), \quad \psi_q(x_1, x_2)|_{q=\pi^-} = \frac{-i\sqrt{3}}{N^2}(-1)^{x_2-x_1}(x_2 - x_1).\quad (22)$$

Two-magnon bound states

The two-magnon scattering matrix for the XXZ chain can be written as [2, 3]

$$\mathcal{S}(q_1, q_2) = \exp[i\Theta(q_1, q_2)] = -\frac{\cos \frac{Q}{2} - \Delta e^{iq}}{\cos \frac{Q}{2} - \Delta e^{-iq}},\quad (23)$$

where $Q = q_1 + q_2$ is the total momentum and $q = (q_1 - q_2)/2$ is the relative momentum.

Bound states correspond to poles of the scattering matrix, which occur when the denominator vanishes,

$$\cos \frac{Q}{2} - \Delta e^{-iq} = 0.\quad (24)$$

For zero total momentum $Q = 0$, we set $p_1 = i\kappa/2$ and $q_2 = -i\kappa/2$ with $\kappa > 0$. The pole condition then yields

$$\Delta e^{-\kappa/2} = 1,\quad (25)$$

leading to

$$\kappa = 2 \ln \Delta.\quad (26)$$

Thus, a two-magnon bound state exists only for $\Delta > 1$.

The corresponding energy eigenvalue is

$$\begin{aligned}\epsilon_2 &= -\frac{N\Delta}{2} + 4 \left(\Delta - \cos \frac{q_1 - q_2}{2} \right) \\ &= -\frac{N\Delta}{2} + 4 \left(\Delta - \cosh \frac{\kappa}{2} \right) \\ &= -\frac{N\Delta}{2} + 2 \left(\Delta - \frac{1}{\Delta} \right).\end{aligned}\quad (27)$$

The corresponding bound-state wavefunction for $x_2 > x_1$ is

$$\psi_{\text{bound}}(x_1, x_2) = A e^{-\ln \Delta (x_2 - x_1)}. \quad (28)$$

The normalization condition

$$\sum_{x_1=1}^N \sum_{x_2=x_1+1}^{x_1+N-1} |\psi_{\text{bound}}(x_1, x_2)|^2 = 1 \quad (29)$$

gives

$$A = \sqrt{\frac{\Delta^2 - 1}{N}}. \quad (30)$$

DERIVATION AND SOLUTION OF THE MASTER EQUATION

Under weak system–bath coupling, the reduced dynamics of the system is described by the second-order time-convolutionless (TCL) master equation. In the interaction picture, the reduced density matrix $\rho_S(t)$ obeys [4]

$$\dot{\rho}_S(t) = - \int_0^t d\tau \Sigma^{(2)}(t, \tau) \rho_S(t), \quad (31a)$$

where the second-order self-energy superoperator is

$$\Sigma^{(2)}(t, \tau) = \text{Tr}_B \left[H_{SB}(t), [H_{SB}(t - \tau), (\cdot) \rho_B] \right]. \quad (31b)$$

Here

$$H_{SB}(t) = e^{i(H_S + H_B)t} H_{SB} e^{-i(H_S + H_B)t}$$

is the system–bath interaction Hamiltonian in the interaction picture, and ρ_B is the equilibrium density matrix of the bath.

We assume a bilinear coupling of the form

$$H_{SB} = S_1 \otimes B_1 + S_2 \otimes B_2,$$

with $S_1 = \sum_i \sigma_i^-$ and $S_2 = \sum_i \sigma_i^+$. Under the Born approximation and assuming an initially factorized state, the master equation can be written as

$$\dot{\rho}_S(t) = S_1(t) \rho_S(t) W_2(t) + S_2(t) \rho_S(t) W_1(t) - W_1(t) S_2(t) \rho_S(t) - W_2(t) S_1(t) \rho_S(t) + \text{H.c.}, \quad (32)$$

where, in the Markov limit, the operators

$$\begin{aligned} W_1(t) &= \int_0^\infty ds S_1(t-s) \Phi_{21}(s), \\ W_2(t) &= \int_0^\infty ds S_2(t-s) \Phi_{12}(s), \end{aligned} \quad (33)$$

are defined in terms of the bath correlation functions.

The system operators admit a block-diagonal representation in the Bethe eigenbasis,

$$\begin{aligned} S_1(t) &= \bigoplus_l \sum_{\mathbf{p}_l, \mathbf{p}'_{l+1}} e^{-it(\epsilon_l - \epsilon_{l+1})} \langle \Psi_{l+1} | \sum_i \sigma_i^- | \Psi_l \rangle | \Psi_{l+1} \rangle \langle \Psi_l |, \\ S_2(t) &= \bigoplus_l \sum_{\mathbf{p}'_l, \mathbf{p}_{l+1}} e^{-it(\epsilon_{l+1} - \epsilon_l)} \langle \Psi_l | \sum_i \sigma_i^+ | \Psi_{l+1} \rangle | \Psi_l \rangle \langle \Psi_{l+1} |. \end{aligned} \quad (34)$$

$$\begin{aligned}
\Phi_{12}(\tau) &= \sum_{k_1, k_2} g_{k_1} g_{k_2} (C_{k_1} + iS_{k_1}) \langle \sigma_{k_1}^- \sigma_{k_2}^+ \rangle = \sum_k g_k^2 (C_k + iS_k) \langle \sigma_k^- \sigma_k^+ \rangle = \gamma \langle e^{2i\omega\tau} p(-\omega) \rangle, \\
\Phi_{21}(\tau) &= \sum_{k_1, k_2} g_{k_1} g_{k_2} (C_{k_1} - iS_{k_1}) \langle \sigma_{k_1}^+ \sigma_{k_2}^- \rangle = \sum_k g_k^2 (C_k - iS_k) \langle \sigma_k^+ \sigma_k^- \rangle = \gamma \langle e^{-2i\omega\tau} p(\omega) \rangle,
\end{aligned} \tag{35}$$

with $\gamma = \sum_k g_k^2$, is a finite positive number dependent on the nature of interaction between the bath spins and the geometrical/spatial arrangements of the spins; $n(\omega)$ is the ensemble spectral density normalized to the total number of spins; $\int d\omega n(\omega) = N_{\text{bath}}$; $p(\omega) = \exp(-\beta\omega)/(2 \cosh(\beta\omega))$ and $\langle f(\omega) \rangle = \int d\omega n(\omega) f(\omega) / \int d\omega n(\omega)$.

Spin systems often possess long-range exchange interactions scaling with distance r as $g_k = C/r^\nu$ with the resonant dipole-dipole interaction, $\nu = 3$, which is the most common case [5]. Let us assume that the bath spins are uniformly scattered in the space with density σ_0 , γ can be computed as follows. In d -dimensional space, the number of particles inside two concentric spheres of radius r and $r + dr$ is $\sigma_0 A_d r^{d-1} dr$, where $A_d = \frac{2\pi^{d/2}}{\Gamma(\frac{d}{2})}$ is the surface area of a d -dimensional sphere of unit radius. Therefore,

$$\gamma = \sum_k g_k^2 = C^2 \sigma_0 A_d \int_a^\infty dr \frac{r^{d-1}}{r^{2\nu}} = C^2 \sigma_0 \frac{2\pi^{d/2}}{\Gamma(\frac{d}{2})} \frac{a^{d-2\nu}}{2\nu - d}, \quad \text{assuming } 2\nu > d. \tag{36}$$

with a being the ultraviolet cutoff length.

Starting from Eqs. (34) and (33), the dissipative operators entering the master equation can be expressed explicitly in the Bethe eigenbasis as

$$\begin{aligned}
W_1(t) &= \frac{\gamma}{N_{\text{bath}}} \bigoplus_{l=0}^N \sum_{\mathbf{p}_l, \mathbf{p}'_{l+1}} e^{-it(\epsilon_l(\mathbf{p}_l) - \epsilon_{l+1}(\mathbf{p}'_{l+1}))} \langle \Psi_{l+1}(\mathbf{p}'_{l+1}) | \sum_i \sigma_i^- | \Psi_l(\mathbf{p}_l) \rangle \\
&\quad \times | \Psi_{l+1}(\mathbf{p}'_{l+1}) \rangle \langle \Psi_l(\mathbf{p}_l) | \int d\omega p(\omega) n(\omega) \mathcal{I}_1(\omega),
\end{aligned} \tag{37}$$

$$\begin{aligned}
W_2(t) &= \frac{\gamma}{N_{\text{bath}}} \bigoplus_{l=0}^N \sum_{\mathbf{p}'_l, \mathbf{p}_{l+1}} e^{-it(\epsilon_{l+1}(\mathbf{p}_{l+1}) - \epsilon_l(\mathbf{p}'_l))} \langle \Psi_l(\mathbf{p}'_l) | \sum_i \sigma_i^+ | \Psi_{l+1}(\mathbf{p}_{l+1}) \rangle \\
&\quad \times | \Psi_l(\mathbf{p}'_l) \rangle \langle \Psi_{l+1}(\mathbf{p}_{l+1}) | \int d\omega p(-\omega) n(\omega) \mathcal{I}_2(\omega).
\end{aligned} \tag{38}$$

Including the Lamb-shift terms, the frequency integrals appearing in Eq. (38) evaluate to

$$\begin{aligned}
\int_{-\infty}^{\infty} d\omega p(\omega) n(\omega) \mathcal{I}_1(\omega) &= \frac{\pi}{2} p\left(\frac{\epsilon_l - \epsilon_{l+1}}{2}\right) n\left(\frac{\epsilon_l - \epsilon_{l+1}}{2}\right) \\
&\quad - i \int_{-\infty}^{\infty} d\omega p(\omega) n(\omega) \mathcal{P}\left(\frac{1}{2\omega - (\epsilon_l - \epsilon_{l+1})}\right),
\end{aligned} \tag{39}$$

$$\begin{aligned}
\int_{-\infty}^{\infty} d\omega p(-\omega) n(\omega) \mathcal{I}_2(\omega) &= \frac{\pi}{2} p\left(\frac{\epsilon_{l+1} - \epsilon_l}{2}\right) n\left(\frac{-\epsilon_{l+1} + \epsilon_l}{2}\right) \\
&\quad + i \int_{-\infty}^{\infty} d\omega p(-\omega) n(\omega) \mathcal{P}\left(\frac{1}{2\omega + (\epsilon_{l+1} - \epsilon_l)}\right),
\end{aligned} \tag{40}$$

where \mathcal{P} denotes the Cauchy principal value.

From Eq. (34) and Eq. (38), the explicit form of the operators are recast as

$$\begin{aligned}
S_1^{01}(t) &= \sqrt{N} e^{-2it(1-\Delta)}, \\
S_2^{10}(t) &= \sqrt{N} e^{2it(1-\Delta)}, \\
W_1^{01}(t) &= \frac{\gamma\sqrt{N}}{N_b} e^{-2it(1-\Delta)} \left[\frac{\pi}{2} p(1-\Delta)n(1-\Delta) - i \int_{-\infty}^{\infty} d\omega p(\omega)n(\omega) \mathcal{P} \left(\frac{1}{2\omega + 2(\Delta-1)} \right) \right], \\
W_2^{10}(t) &= \frac{\gamma\sqrt{N}}{N_b} e^{2it(1-\Delta)} \left[\frac{\pi}{2} p(\Delta-1)n(1-\Delta) + i \int_{-\infty}^{\infty} d\omega p(-\omega)n(\omega) \mathcal{P} \left(\frac{1}{2\omega + 2(\Delta-1)} \right) \right].
\end{aligned} \tag{41}$$

Reduced dynamics of zero magnon sector

Restricting to the zero- and one-magnon sectors, the reduced density matrix in the Bethe eigenbasis reads

$$\begin{aligned}
\rho(t) &= \rho_{00}(t)|\Psi_0\rangle\langle\Psi_0| + \rho_{01}(t)|\Psi_0\rangle\langle\Psi_1(\mathbf{p}=0)| \\
&\quad + \rho_{01}^*(t)|\Psi_1(\mathbf{p}=0)\rangle\langle\Psi_0| + \rho_{11}(t)|\Psi_1(\mathbf{p}=0)\rangle\langle\Psi_1(\mathbf{p}=0)| + \dots
\end{aligned} \tag{42}$$

In this truncated basis, the operators $S_1(t)$, $S_2(t)$, $W_1(t)$, and $W_2(t)$ reduce to

$$\begin{aligned}
S_1(t) &= \begin{pmatrix} 0 & S_1^{01}(t) \\ 0 & 0 \end{pmatrix}, & S_2(t) &= \begin{pmatrix} 0 & 0 \\ S_2^{10}(t) & 0 \end{pmatrix}, \\
W_1(t) &= \begin{pmatrix} 0 & W_1^{01}(t) \\ 0 & 0 \end{pmatrix}, & W_2(t) &= \begin{pmatrix} 0 & 0 \\ W_2^{10}(t) & 0 \end{pmatrix}.
\end{aligned} \tag{43}$$

The master equation Eq. (32) then simplifies to

$$\begin{pmatrix} \dot{\rho}_{00} & \dot{\rho}_{01} \\ \dot{\rho}_{01}^* & \dot{\rho}_{11} \end{pmatrix} = \begin{pmatrix} S_1^{01}\rho_{11}W_2^{10} - W_1^{01}\rho_{00}S_2^{10} + \text{h.c.} & W_1^{01}\rho_{01}S_2^{10} + \text{h.c.} \\ W_2^{10}\rho_{01}^*S_1^{01} + \text{h.c.} & S_2^{10}\rho_{00}W_1^{01} - W_2^{10}\rho_{11}S_1^{01} + \text{h.c.} \end{pmatrix}. \tag{44}$$

The evolution of the coherence $\rho_{01}(t)$ is governed by

$$\dot{\rho}_{01}(t) = W_1^{01}(t)\rho_{01}(t)S_2^{10}(t) + W_1^{*01}(t)\rho_{01}^*(t)S_2^{*10}(t). \tag{45}$$

Separating real and imaginary parts and imposing the initial conditions $\text{Re}[\rho_{01}(0)] = \text{Im}[\rho_{01}(0)] = 0$, we obtain

$$\text{Re}[\rho_{01}(t)] = 0, \quad \text{Im}[\rho_{01}(t)] = 0. \tag{46}$$

Thus, coherences are not dynamically generated in this truncated subspace.

The population dynamics are given by

$$\dot{\rho}_{00}(t) = S_1^{01}\rho_{11}W_2^{10} - W_1^{01}\rho_{00}S_2^{10} + \text{h.c.}, \tag{47}$$

$$\dot{\rho}_{11}(t) = S_2^{10}\rho_{00}W_1^{01} - W_2^{10}\rho_{11}S_1^{01} + \text{h.c.}. \tag{48}$$

Using $\rho_{00}(t) + \rho_{11}(t) = 1$, we obtain a closed equation for $\rho_{11}(t)$:

$$\dot{\rho}_{11}(t) = (S_2^{10}W_1^{01} + S_2^{*10}W_1^{*01}) - \rho_{11}(t) (S_2^{10}W_1^{01} + W_2^{10}S_1^{01} + S_2^{*10}W_1^{*01} + W_2^{*10}S_1^{*01}). \tag{49}$$

$$\implies \rho_{11}(t) = 1 - \frac{\text{Re}[S_2^{10}W_1^{01}]}{\text{Re}[S_2^{10}W_1^{01} + W_2^{10}S_1^{01}]} (1 - e^{-2t(\text{Re}[S_2^{10}W_1^{01} + W_2^{10}S_1^{01}])}). \tag{50}$$

Decay of extremal coherences: $|\Psi_0\rangle\langle\Psi_N|$ sector

We consider an initial coherence between the fully polarized ferromagnetic states, $\rho(0) = |\Psi_0\rangle\langle\Psi_N|$. Under the system–bath dynamics generated by Eq. (32), the reduced density matrix at time t is confined to the subspace $\{|\Psi_0\rangle, |\Psi_1\rangle, |\Psi_{N-1}\rangle, |\Psi_N\rangle\}$

and can be written as

$$\rho(t) = \rho_{0N}(t)|\Psi_0\rangle\langle\Psi_N| + \rho_{0,N-1}(t)|\Psi_0\rangle\langle\Psi_{N-1}| + \rho_{1,N-1}(t)|\Psi_1\rangle\langle\Psi_{N-1}| + \rho_{1N}(t)|\Psi_1\rangle\langle\Psi_N|. \quad (51)$$

In the ordered Bethe basis $\{|\Psi_0\rangle, |\Psi_1\rangle, |\Psi_{N-1}\rangle, |\Psi_N\rangle\}$, the operators $S_{1,2}(t)$ and $W_{1,2}(t)$ take the block form

$$\begin{aligned} S_1(t) &= \begin{pmatrix} 0 & S_1^{01}(t) & 0 & 0 \\ 0 & 0 & 0 & 0 \\ 0 & 0 & 0 & S_1^{N-1,N}(t) \\ 0 & 0 & 0 & 0 \end{pmatrix}, & S_2(t) &= \begin{pmatrix} 0 & 0 & 0 & 0 \\ S_2^{10}(t) & 0 & 0 & 0 \\ 0 & 0 & 0 & 0 \\ 0 & 0 & S_2^{N,N-1}(t) & 0 \end{pmatrix}, \\ W_1(t) &= \begin{pmatrix} 0 & W_1^{01}(t) & 0 & 0 \\ 0 & 0 & 0 & 0 \\ 0 & 0 & 0 & W_1^{N-1,N}(t) \\ 0 & 0 & 0 & 0 \end{pmatrix}, & W_2(t) &= \begin{pmatrix} 0 & 0 & 0 & 0 \\ W_2^{10}(t) & 0 & 0 & 0 \\ 0 & 0 & 0 & 0 \\ 0 & 0 & W_2^{N,N-1}(t) & 0 \end{pmatrix}. \end{aligned} \quad (52)$$

Projecting Eq. (32) onto this subspace yields

$$\begin{pmatrix} 0 & 0 & \dot{\rho}_{0,N-1} & \dot{\rho}_{0N} \\ 0 & 0 & \dot{\rho}_{1,N-1} & \dot{\rho}_{1N} \\ \dot{\rho}_{0,N-1}^* & \dot{\rho}_{1,N-1}^* & 0 & 0 \\ \dot{\rho}_{0N}^* & \dot{\rho}_{1N}^* & 0 & 0 \end{pmatrix} = \begin{pmatrix} 0 & 0 & A_{0,N-1} & A_{0N} \\ 0 & 0 & A_{1,N-1} & A_{1N} \\ A_{N-1,0} & A_{N-1,1} & 0 & 0 \\ A_{N,0} & A_{N,1} & 0 & 0 \end{pmatrix} + \text{h.c.} \quad (53)$$

with

$$\begin{aligned} A_{0,N-1} &= W_2^{N,N-1} \rho_{1N} S_1^{01} - W_1^{01} \rho_{0,N-1} S_2^{10}, \\ A_{0N} &= -W_1^{01} \rho_{0N} S_2^{10}, \\ A_{1,N-1} &= -W_2^{10} \rho_{1,N-1} S_1^{01}, \\ A_{1N} &= W_1^{N-1,N} \rho_{0,N-1} S_2^{10} - W_2^{10} \rho_{1N} S_1^{01}, \end{aligned} \quad (54)$$

and Hermitian conjugates defining the remaining entries.

Using spin-flip symmetry of the XXZ Hamiltonian,

$$\begin{aligned} S_1^{01} &= S_2^{N,N-1}, & S_2^{10} &= S_1^{N-1,N}, \\ W_1^{01} &= W_2^{N,N-1}, & W_2^{10} &= W_1^{N-1,N}, \end{aligned} \quad (55)$$

the equations for the extremal coherences $(0, N)$ and $(1, N-1)$ decouple.

From the $(1, 4)$ and $(4, 1)$ components we obtain

$$\begin{aligned} \dot{\rho}_{0N} &= -W_1^{01} S_2^{10} \rho_{0N} - W_1^{*01} S_2^{*10} \rho_{0N}^*, \\ \dot{\rho}_{0N}^* &= -W_1^{01} S_2^{10} \rho_{0N}^* - W_1^{*01} S_2^{*10} \rho_{0N}. \end{aligned} \quad (56)$$

Separating real and imaginary parts,

$$\begin{aligned} \text{Re}[\dot{\rho}_{0N}] &= -2 \text{Re}(W_1^{01} S_2^{10}) \text{Re}[\rho_{0N}], \\ \text{Im}[\dot{\rho}_{0N}] &= 0, \end{aligned} \quad (57)$$

leading to the exponential decay

$$\text{Re}[\rho_{0N}(t)] = \text{Re}[\rho_{0N}(0)] \exp[-2t \text{Re}(W_1^{01} S_2^{10})]. \quad (58)$$

Analogously, from the $(2, 3)$ and $(3, 2)$ components,

$$\text{Re}[\rho_{1,N-1}(t)] = \text{Re}[\rho_{1,N-1}(0)] \exp[-2t \text{Re}(W_2^{10} S_1^{01})], \quad \text{Im}[\rho_{1,N-1}(t)] = 0. \quad (59)$$

Reduced Dynamics of the generalized W state

From Eqs. (34) and (38), the explicit forms of the transition operators coupling the one-magnon and two-magnon sectors can be written as

$$\begin{aligned}
S_1^{12}(q, t) &= \Omega_q^* e^{-2it(2 \cos q - 1 - 2\Delta)}, \\
S_2^{21}(q, t) &= \Omega_q e^{2it(2 \cos q - 1 - 2\Delta)}, \\
W_1^{12}(q, t) &= \frac{\gamma \Omega_q^*}{N_b} e^{-2it(2 \cos q - 1 - 2\Delta)} \left[\frac{\pi}{2} p(2 \cos q - 1 - \Delta) n(2 \cos q - 1 - \Delta) \right. \\
&\quad \left. - i \int_{-\infty}^{\infty} d\omega p(\omega) n(\omega) \mathcal{P} \left(\frac{1}{2\omega + 2\Delta + 2 - 4 \cos q} \right) \right], \\
W_2^{21}(q, t) &= \frac{\gamma \Omega_q}{N_b} e^{2it(2 \cos q - 1 - 2\Delta)} \left[\frac{\pi}{2} p(1 + \Delta - 2 \cos q) n(2 \cos q - 1 - \Delta) \right. \\
&\quad \left. + i \int_{-\infty}^{\infty} d\omega p(-\omega) n(\omega) \mathcal{P} \left(\frac{1}{2\omega + 2\Delta + 2 - 4 \cos q} \right) \right].
\end{aligned}$$

Here \mathcal{P} denotes the Cauchy principal value.

The transition amplitude Ω_q is obtained from the two-magnon scattering and bound-state wavefunctions, Eqs. (17), (22), and (28),

$$\Omega_q = \langle \Psi_1 | \sum_i \sigma_i^+ | \Psi_2(q) \rangle = \frac{2}{\sqrt{N}} \sum_{x_1=1}^N \sum_{x_2=x_1+1}^{x_1+N-1} \psi_q(x_1, x_2) = \mathcal{O} \left(\frac{1}{\sqrt{N}} \right), \quad (60)$$

for generic momenta q .

However, near the band edges the overlap is enhanced,

$$\begin{aligned}
\lim_{q \rightarrow 0^+} \Omega_q &= -i\sqrt{3N}, \\
\lim_{q \rightarrow \pi^-} \Omega_q &= +i\sqrt{3N},
\end{aligned} \quad (61)$$

indicating a collective enhancement of the transition matrix element. For the two-magnon bound state,

$$\Omega_{\text{bound}} = \langle \Psi_1 | \sum_i \sigma_i^+ | \Psi_2(\text{bound}) \rangle = 2\sqrt{\frac{\Delta+1}{\Delta-1}}, \quad (62)$$

which remains $\mathcal{O}(1)$ in the thermodynamic limit.

Retaining only the dominant modes $\{|\Psi_0\rangle, |\Psi_1(q=0)\rangle, |\Psi_2(q=0^+)\rangle, |\Psi_2(q=\pi^-)\rangle\}$, the master equation (32) reduces to

$$\dot{\rho}(t) = \mathcal{M}(\beta, \Delta) \rho(t). \quad (63)$$

Within the secular approximation, the density matrix remains diagonal in this basis,

$$\rho(t) = \begin{pmatrix} w_0 & 0 & 0 & 0 \\ 0 & w_1 & 0 & 0 \\ 0 & 0 & w_2(0^+) & 0 \\ 0 & 0 & 0 & w_2(\pi^-) \end{pmatrix}. \quad (64)$$

The Markov generator takes the form

$$\mathcal{M}(\beta, \Delta) = \begin{pmatrix} -S_2^{10} W_1^{01} & S_1^{01} W_2^{10} & 0 & 0 \\ S_2^{10} W_1^{01} & -\sum_{q=0^+, \pi^-} S_2^{21}(q) W_1^{12}(q) - S_1^{01} W_2^{10} & S_1^{12}(0^+) W_2^{21}(0^+) & S_1^{12}(\pi^-) W_2^{21}(\pi^-) \\ 0 & S_2^{21}(0^+) W_1^{12}(0^+) & -S_1^{12}(0^+) W_2^{21}(0^+) & 0 \\ 0 & S_2^{21}(\pi^-) W_1^{12}(\pi^-) & 0 & -S_1^{12}(\pi^-) W_2^{21}(\pi^-) \end{pmatrix}. \quad (65)$$

By construction, $\sum_i \dot{w}_i = 0$, ensuring probability conservation.

One of the eigenvalues of the matrix $\mathcal{M}(\beta, \Delta)$ is zero and the rest three eigenvalues are determined from the following cubic equation

$$\lambda^3 + (a_1 + a_2 + a_3 + b_1 + b_2 + b_3)\lambda^2 + (a_1a_2 + a_1a_3 + a_2a_3 + a_1(b_2 + b_3) + a_2(b_1 + b_3) + a_3(b_1 + b_2))\lambda + (a_1a_2b_3 + a_1a_3b_2 + a_2a_3b_1) = 0, \quad (66)$$

and the corresponding eigenvectors are of the form

$$\mathbf{v}^{(\lambda)} = \begin{pmatrix} b_1 \\ \frac{b_1}{a_1 + \lambda} \\ 1 \\ \frac{b_2}{a_2 + \lambda} \\ b_3 \\ \frac{b_3}{a_3 + \lambda} \end{pmatrix}, \quad (67)$$

where

$$\begin{aligned} a_1 &= S_2^{10}W_1^{01}, \\ a_2 &= S_1^{12}(0^+)W_2^{21}(0^+), \\ a_3 &= S_1^{12}(\pi^-)W_2^{21}(\pi^-), \\ b_1 &= S_1^{01}W_2^{10}, \\ b_2 &= S_2^{21}(0^+)W_1^{12}(0^+), \\ b_3 &= S_2^{21}(\pi^-)W_1^{12}(\pi^-). \end{aligned} \quad (68)$$

The time-dependent population vector $\mathbf{w}(t) \equiv (w_0(t), w_1(t), w_2(0^+)(t), w_2(\pi^-)(t))$ can therefore be written as

$$\mathbf{w}(t) = \sum_{\lambda} e^{\lambda t} c_{\lambda} \mathbf{v}^{(\lambda)}, \quad \text{where} \quad \mathbf{w}(0) = \sum_{\lambda} c_{\lambda} \mathbf{v}^{(\lambda)}. \quad (69)$$

DISTILLATION PROTOCOL FOR THE GENERALIZED GHZ STATE

GHZ distillation via bilateral CNOT and postselection

We briefly summarize the standard multipartite GHZ distillation protocol [6]. A general n -qubit state is written as

$$\rho = \sum_{x,y \in \{0,1\}^n} \rho_{x,y} |x\rangle\langle y|. \quad (70)$$

Step 1: Bilateral CNOT operation. Two identical copies of the state are prepared, labeled as control (C) and target (T). Each of the n parties applies a local CNOT gate, with the control qubit acting on the corresponding target qubit. The global unitary thus maps

$$|x\rangle_C |u\rangle_T \mapsto |x\rangle_C |u \oplus x\rangle_T, \quad (71)$$

where \oplus denotes bitwise XOR. This operation correlates phase information in the control copy with bit-flip information in the target copy.

Step 2: Collective parity measurement. After the CNOT layer, the target register is measured collectively by projecting onto the subspace spanned by $|0\rangle^{\otimes n}$ and $|1\rangle^{\otimes n}$. Only successful measurement outcomes are retained. Tracing out the target system

yields a post-selected control state,

$$\rho^{(1)} = \frac{\text{Tr}_T[(\mathbb{I}_C \otimes P_T) U(\rho^{\otimes 2}) U^\dagger (\mathbb{I}_C \otimes P_T)]}{p_1}, \quad (72)$$

where p_1 is the corresponding success probability. This step suppresses bit-flip errors while preserving GHZ-type coherence.

Step 3: Iteration and hashing. The above procedure can be iterated r times, producing a sequence of post-selected states with success probabilities $\{p_i\}$. After sufficient purification, a multipartite hashing protocol is applied. This yields a lower bound on the distillable GHZ entanglement,

$$\mathcal{E}_D^{\text{GHZ}} \geq \max_{r \geq 0} \left[R_{\text{hash}}(r) \prod_{i=1}^r p_i \right], \quad (73)$$

where the hashing rate is

$$R_{\text{hash}} = 1 - H(P_\mu) - H(P_\nu). \quad (74)$$

Step 4: GHZ stabilizer representation. Here $P_{\mu\nu} = \langle \mu\nu | \rho | \mu\nu \rangle$ are populations in the GHZ stabilizer basis

$$|\mu\nu\rangle = \frac{1}{\sqrt{2}} (|\mu, 0\rangle + (-1)^\nu |\mu, \overline{0}\rangle), \quad (75)$$

with $\mu \in \{0, 1\}^{n-1}$ labeling phase errors and $\nu \in \{0, 1\}$ labeling bit-flip errors. The quantities $H(P_\mu)$ and $H(P_\nu)$ are the corresponding Shannon entropies of the marginal distributions.

Operationally, the bilateral CNOT and postselection steps convert multipartite phase correlations into detectable parity information. The hashing stage extracts asymptotically perfect GHZ states at a finite rate whenever the total entropy lies below the stabilizer threshold.

GHZ distillation protocol for the Bethe-basis reduced state

The input state for the recurrence protocol, expressed in the restricted Bethe basis $\{|\Psi_0\rangle, |\Psi_1(q=0)\rangle, |\Psi_{N-1}(q=0)\rangle, |\Psi_N\rangle\}$, has the block-diagonal form

$$\rho^{(0)} = \begin{pmatrix} \frac{u}{2} & 0 & 0 & v \\ 0 & \frac{w}{2} & 0 & 0 \\ 0 & 0 & \frac{w}{2} & 0 \\ v^* & 0 & 0 & \frac{u}{2} \end{pmatrix}, \quad (76)$$

where $u, w \geq 0$ and $v \in \mathbb{C}$, with $\text{Tr } \rho^{(0)} = 1$.

The distillation step follows a standard multipartite recurrence protocol [7, 8]. Two identical copies of the state are taken, one as the control and the other as the target. Each party applies a local CNOT gate from control to target, followed by a global projective measurement on the target register onto the subspace spanned by $|0\rangle^{\otimes N}$ and $|1\rangle^{\otimes N}$. Successful outcomes are post-selected, yielding a renormalized control state.

In the Bethe basis, the action of the global CNOT operation simplifies considerably. The product states $|0\rangle^{\otimes N}$ and $|1\rangle^{\otimes N}$ are mapped deterministically, while the one- and $(N-1)$ -excitation sectors contribute suppressed amplitudes by $1/\sqrt{N}$. Repeated post-selection progressively filters out the Dicke type states, in large- N many-body systems.

Recurrence relations

After one successful iteration, the unnormalized density matrix $\sigma_{(l+1)}$ retains the same block structure as $\rho_{(l)}$, with coefficients obeying

$$u_{l+1} = u_l^2, \quad (77)$$

$$w_{l+1} = \frac{w_l^2}{N}, \quad (78)$$

$$v_{l+1} = v_l^2 + |v_l|^2. \quad (79)$$

In the thermodynamic limit $N \rightarrow \infty$, the Dicke contribution w_l is exponentially suppressed and can be neglected. The remaining coefficients evolve as

$$u_r = u^{2^r}, \quad (80)$$

$$v_r = 2^{2^r - 1} (\text{Re } v)^{2^r - 1} v. \quad (81)$$

The success probability at $(l + 1)$ th iteration is

$$p_{l+1} = \text{Tr } \sigma_{(l+1)} = 2u_l^2, \quad (82)$$

leading to the cumulative probability

$$\prod_{i=1}^r p_i = u^{2^{r+1} - 2}. \quad (83)$$

After normalization, the control state at the r th iteration approaches the GHZ-diagonal form

$$\rho^{(r)} = \begin{pmatrix} \frac{1}{2} & 0 & 0 & v_r \\ 0 & 0 & 0 & 0 \\ 0 & 0 & 0 & 0 \\ v_r^* & 0 & 0 & \frac{1}{2} \end{pmatrix}. \quad (84)$$

GHZ stabilizer projections and rate

Only two GHZ stabilizer basis states contribute non-vanishing weights,

$$(\mu, \nu) = (0 \dots 0, 0), (0 \dots 0, 1).$$

Their probabilities are

$$P_{0 \dots 0, 0}^{(r)} = \frac{1}{2} \left[1 + (2 \text{Re } v)^{2^r} \right], \quad (85)$$

$$P_{0 \dots 0, 1}^{(r)} = \frac{1}{2} \left[1 - (2 \text{Re } v)^{2^r} \right]. \quad (86)$$

Thus, $P_\mu^{(r)} = 1$, and $P_\nu^{(r)} = \{P_0^{(r)}, P_1^{(r)}\}$.

Following [7, 9], the achievable lower bound on the distillable GHZ entanglement is

$$\mathcal{E}_D^{\text{GHZ}} = \max_{r \geq 0} \left[u^{2^{r+1} - 2} \left(1 - h \left(P_0^{(r)}, P_1^{(r)} \right) \right) \right], \quad (87)$$

where h denotes the binary Shannon entropy.

This expression highlights the competition between exponential purification of GHZ coherence and the exponentially decreasing success probability, which together determine the optimal distillation.

GEOMETRIC MEASURE FOR MULTIPARTITE ENTANGLEMENT FOR THE GENERALIZED GHZ STATE AND THE GENERALIZED W STATE

GME for the evolved GHZ state

The geometric measure of genuine multipartite entanglement (GME) for a pure N -qubit state $|\psi\rangle$ is defined as [10]

$$E_G(|\psi\rangle) \equiv 1 - \Lambda(|\psi\rangle), \quad (88)$$

where

$$\Lambda(|\psi\rangle) \equiv \max_{|\phi\rangle \in \text{BS}} |\langle \phi | \psi \rangle|^2, \quad (89)$$

and BS denotes the set of all pure biseparable states over all possible bipartitions of the N parties. For pure states, E_G satisfies all axioms of a genuine multipartite entanglement monotone [10, 11].

For a mixed state ρ , the geometric measure is extended via the convex-roof construction [10, 12, 13]

$$E_G(\rho) = \inf_{\{p_i, |\psi_i\rangle\}} \sum_i p_i E_G(|\psi_i\rangle), \quad \rho = \sum_i p_i |\psi_i\rangle \langle \psi_i|. \quad (90)$$

We consider a class of N -qubit mixed states on a restricted Bethe basis $\{|\Psi_0\rangle, |\Psi_1(q=0)\rangle, |\Psi_{N-1}(q=0)\rangle, |\Psi_N\rangle\}$, with density matrix

$$\rho = \begin{pmatrix} \frac{u}{2} & 0 & 0 & v \\ 0 & \frac{1-u}{2} & 0 & 0 \\ 0 & 0 & \frac{1-u}{2} & 0 \\ v & 0 & 0 & \frac{u}{2} \end{pmatrix}, \quad 0 \leq u \leq 1. \quad (91)$$

Due to orthogonality of different magnon-number sectors, ρ admits a convex decomposition into three mutually orthogonal components: (i) the zero- and N -magnon sector, (ii) the one-magnon sector, and (iii) the $(N-1)$ -magnon sector. Explicitly,

$$\rho = u \rho_{0N} + \frac{1-u}{2} \rho_1 + \frac{1-u}{2} \rho_{N-1}, \quad (92)$$

where

$$\rho_{0N} = \begin{pmatrix} \frac{1}{2} & \frac{v}{u} \\ \frac{v^*}{u} & \frac{1}{2} \end{pmatrix}, \quad (93)$$

$$\rho_1 = |\Psi_1(q=0)\rangle \langle \Psi_1(q=0)|, \quad (94)$$

$$\rho_{N-1} = |\Psi_{N-1}(q=0)\rangle \langle \Psi_{N-1}(q=0)|. \quad (95)$$

Since these sectors are supported on mutually orthogonal subspaces, the convex-roof optimization can be analyzed sector-wise. In particular, the geometric GME of ρ is determined by the entanglement properties of the GHZ-like ρ_{0N} block and the Dicke-type one- and $(N-1)$ -magnon states, which are known to possess genuine multipartite entanglement.

Geometric GME of the ρ_{0N} block

We consider the normalized zero- N magnon block

$$\rho_{0N} = \begin{pmatrix} \frac{1}{2} & \frac{v}{u} \\ \frac{v}{u} & \frac{1}{2} \end{pmatrix}, \quad |v| \leq \frac{u}{2}, \quad (96)$$

written in the basis $\{|\Psi_0\rangle, |\Psi_N\rangle\} = \{|0\rangle^{\otimes N}, |1\rangle^{\otimes N}\}$. This state is supported entirely in the GHZ subspace. Any pure state in this subspace can be parameterized as

$$|\psi(\theta, \phi)\rangle = \cos \theta |\Psi_0\rangle + e^{i\phi} \sin \theta |\Psi_N\rangle, \quad 0 \leq \theta \leq \frac{\pi}{2}. \quad (97)$$

For such states, the maximal overlap with the set of biseparable states is attained by product states aligned with either $|\Psi_0\rangle$ or $|\Psi_N\rangle$. Hence

$$\Lambda(|\psi\rangle) = \max_{|\phi\rangle \in \text{BS}} |\langle \phi | \psi \rangle|^2 = \max\{\cos^2 \theta, \sin^2 \theta\}. \quad (98)$$

The geometric measure of genuine multipartite entanglement is therefore

$$E_G(|\psi\rangle) = 1 - \Lambda(|\psi\rangle) = \min\{\cos^2 \theta, \sin^2 \theta\} = \frac{1}{2} (1 - |\cos 2\theta|). \quad (99)$$

The eigenvalues of the state in Eq. (96) are

$$\lambda_{\pm} = \frac{1}{2} \left(1 \pm \sqrt{1 - \frac{4v^2}{u^2}} \right). \quad (100)$$

The geometric GME for mixed states is defined via the convex roof

$$E_G(\rho_{0N}) = \inf_{\{p_i, |\psi_i\rangle\}} \sum_i p_i E_G(|\psi_i\rangle), \quad \rho_{0N} = \sum_i p_i |\psi_i\rangle \langle \psi_i|. \quad (101)$$

Let $|\psi_i\rangle$ be pure states of the form $|\psi(\theta_i, \phi_i)\rangle$. Using Eq. (99), we have

$$\sum_i p_i E_G(|\psi_i\rangle) = \frac{1}{2} \sum_i p_i (1 - |\cos 2\theta_i|). \quad (102)$$

The function $f(x) = |x|$ is convex. Hence, by Jensen inequality,

$$\sum_i p_i |\cos 2\theta_i| \geq \left| \sum_i p_i \cos 2\theta_i \right|. \quad (103)$$

Substituting Eq. (103) into Eq. (102), we obtain

$$\sum_i p_i E_G(|\psi_i\rangle) \geq \frac{1}{2} \left(1 - \left| \sum_i p_i \cos 2\theta_i \right| \right). \quad (104)$$

The x -component of the Bloch vector of ρ_{0N} is

$$\frac{2|v|}{u} = \sum_i p_i \sin 2\theta_i \cos \phi_i. \quad (105)$$

Since $|\cos \phi_i| \leq 1$, the Cauchy–Schwarz inequality implies

$$\left| \sum_i p_i \sin 2\theta_i \cos \phi_i \right| \leq \sum_i p_i |\sin 2\theta_i|. \quad (106)$$

Using $\sin^2 2\theta_i + \cos^2 2\theta_i = 1$, the constraint yields

$$\left| \sum_i p_i \cos 2\theta_i \right| = \sqrt{1 - \frac{4v^2}{u^2}}. \quad (107)$$

Equality is achieved by a symmetric decomposition into two pure states with phases $\phi = 0, \pi$.

Substituting Eq. (107) into Eq. (104), we obtain

$$E_G(\rho_{0N}) = \frac{1}{2} \left(1 - \sqrt{1 - \frac{4v^2}{u^2}} \right). \quad (108)$$

The result is independent of system size N because ρ_{0N} is supported entirely within the GHZ subspace. The convex-roof minimum is computed by a two-element ensemble, consistent with general results for rank-2 states.

Geometric entanglement of W states

Geometric collective multipartite entanglement: For permutation-invariant states such as the generalized W state, the maximal overlap is achieved by symmetric product states [14]. Thus it suffices to consider product states of the form

$$|\phi(\theta)\rangle = (\cos\theta |0\rangle + \sin\theta |1\rangle)^{\otimes N}, \quad 0 \leq \theta \leq \frac{\pi}{2}. \quad (109)$$

The overlap between $|\Psi_1(q=0)\rangle$ and $|\phi(\theta)\rangle$ is

$$\langle\phi(\theta)|\Psi_1(q=0)\rangle\langle\phi(\theta)|\Psi_1(q=0)\rangle = \frac{1}{\sqrt{N}} \sum_{j=1}^N \sin\theta (\cos\theta)^{N-1} = \sqrt{N} \sin\theta (\cos\theta)^{N-1}. \quad (110)$$

Hence

$$|\langle\phi(\theta)|\Psi_1(q=0)\rangle\langle\phi(\theta)|\Psi_1(q=0)\rangle|^2 = N \sin^2\theta (\cos^2\theta)^{N-1}. \quad (111)$$

To maximize this expression, we differentiate with respect to θ :

$$\frac{d}{d\theta} [\ln(\sin^2\theta (\cos^2\theta)^{N-1})] = 2 \cot\theta - 2(N-1) \tan\theta = 0. \quad (112)$$

This yields the optimal angle

$$\sin^2\theta = \frac{1}{N}, \quad \cos^2\theta = \frac{N-1}{N}. \quad (113)$$

Substituting Eq. (113) into Eq. (111), we obtain

$$\Lambda(|\Psi_1(q=0)\rangle) = \left(\frac{N-1}{N}\right)^{N-1}. \quad (114)$$

Therefore, the geometric measure of genuine multipartite entanglement is

$$E_G(|\Psi_1(q=0)\rangle) = 1 - \left(\frac{N-1}{N}\right)^{N-1}. \quad (115)$$

In the thermodynamic limit,

$$\lim_{N \rightarrow \infty} \left(\frac{N-1}{N}\right)^{N-1} = e^{-1}, \quad (116)$$

we obtain

$$\lim_{N \rightarrow \infty} E_G(|\Psi_1(q=0)\rangle) = 1 - \frac{1}{e} \approx 0.6321. \quad (117)$$

The maximization over fully separable states suffices because of permutation symmetry and the convexity of the biseparable set. Unlike GHZ states, whose geometric GME is $1/2$ independent of N , the W state exhibits a strictly larger and size-dependent GME. The finite asymptotic value reflects the robustness of W -type entanglement under particle loss.

Geometric genuine multipartite entanglement: We consider a bipartition $A|B$ with $|A| = m$ and $|B| = N - m$. Separating the sum according to whether the excitation lies in A or in B , the state can be written as

$$|\Psi_1(q=0)\rangle \equiv |W_N\rangle = \frac{1}{\sqrt{N}} \left(\sum_{i \in A} |i\rangle_A |0\rangle_B + \sum_{j \in B} |0\rangle_A |j\rangle_B \right). \quad (118)$$

Define the normalized states

$$|W_m\rangle_A = \frac{1}{\sqrt{m}} \sum_{i \in A} |i\rangle_A, \quad |W_{N-m}\rangle_B = \frac{1}{\sqrt{N-m}} \sum_{j \in B} |j\rangle_B. \quad (119)$$

Then the state becomes

$$|W_N\rangle = \sqrt{\frac{m}{N}} |W_m\rangle_A |0\rangle_B + \sqrt{\frac{N-m}{N}} |0\rangle_A |W_{N-m}\rangle_B. \quad (120)$$

The two terms above are orthogonal because they belong to different excitation-number sectors of subsystem A : the first term has one excitation in A , whereas the second has zero excitations in A . Therefore the decomposition is already in Schmidt form. The corresponding Schmidt coefficients are

$$\lambda_1^2 = \frac{m}{N}, \quad \lambda_2^2 = \frac{N-m}{N}. \quad (121)$$

The largest Schmidt coefficient for a fixed bipartition is

$$\lambda_{\max}^2(A|B) = \max\left(\frac{m}{N}, \frac{N-m}{N}\right). \quad (122)$$

We now maximize over all possible bipartitions, i.e. over $m = 1, 2, \dots, N-1$. Since $\max(m, N-m)$ is largest when one subsystem contains a single site, the global maximum is achieved at $m = 1$ (or equivalently $m = N-1$), yielding

$$\lambda_{\max}^2 = \frac{N-1}{N}. \quad (123)$$

Using the definition of the geometric measure of GME we obtain

$$E_G(|\Psi_1(q=0)\rangle) = 1 - \frac{N-1}{N} = \frac{1}{N}. \quad (124)$$

Geometric entanglement of the two-magnon sector

Geometric collective multipartite entanglement: We consider the normalized two-magnon state on a periodic chain,

$$|\Psi_2(q=0)\rangle = \sum_{x_1, x_2} \frac{\sqrt{3}}{N^2} (x_2 - x_1) |x_1, x_2\rangle, \quad (125)$$

which is translationally invariant in the thermodynamic limit. The state $|\Psi_2(q=0)\rangle$ defined in Eq. (125) is not fully permutation invariant due to the position-dependent weight $(x_2 - x_1)$. However, the restriction follows from a variational argument as follows. We consider a general ansatz product state [14]

$$|\phi\rangle = \bigotimes_{k=1}^N (\alpha_k |0\rangle + \beta_k |1\rangle), \quad |\alpha_k|^2 + |\beta_k|^2 = 1. \quad (126)$$

The overlap reads

$$\langle \phi | \Psi_2(q=0) \rangle = \frac{\sqrt{3}}{N^2} \sum_{x_1, x_2} (x_2 - x_1) \beta_{x_1} \beta_{x_2} \prod_{k \neq x_1, x_2} \alpha_k = \frac{\sqrt{3}}{N^2} P \sum_{x_1, x_2} (x_2 - x_1) \frac{\beta_{x_1}}{\alpha_{x_2}} \frac{\beta_{x_2}}{\alpha_{x_1}}, \quad (127)$$

where $P = \prod_{k=1}^N \alpha_k$. Introducing the variables $z_k = \frac{\beta_k}{\alpha_k}$, $\alpha_k = (1 + z_k^2)^{-1/2}$ we get

$$P = \prod_{k=1}^N \frac{1}{\sqrt{1 + z_k^2}}, \quad (128)$$

and the overlap becomes

$$F(\{z_k\}) = \frac{\sqrt{3}}{N^2} \left(\prod_{k=1}^N \frac{1}{\sqrt{1 + z_k^2}} \right) \sum_{x_1, x_2} (x_2 - x_1) z_{x_1} z_{x_2}. \quad (129)$$

By defining the symmetric matrix

$$K_{ij} = \begin{cases} |i - j|, & i \neq j, \\ 0, & i = j. \end{cases} \quad (130)$$

we obtain the following functional

$$F_N(z_1, \dots, z_N) = \frac{\sum_{i,j} K_{ij} z_i z_j}{N \prod_{k=1}^N \sqrt{1 + z_k^2}}, \quad (131)$$

where, K is real, symmetric, and circulant (defined over a periodic boundary condition), $K_{ij} = f(i - j)$ with periodic boundary conditions, $K_{ij} \geq 0$. Our goal is to determine the configuration (z_1, \dots, z_N) that maximizes F_N in the thermodynamic limit.

Since K is circulant, it is diagonalized by discrete Fourier modes:

$$z_j = \sum_q c_q e^{iqj}, \quad (132)$$

where $q = 2\pi n/N$. Then

$$z^T K z = N \sum_q \lambda(q) |c_q|^2, \quad (133)$$

where $\lambda(q)$ is the Fourier transform of f . Because $K_{ij} \geq 0$, its Fourier transform satisfies [15]

$$\lambda(0) > \lambda(q) \quad \text{for } q \neq 0. \quad (134)$$

Therefore the numerator in Eq. (131) is maximized when, $z_j = \text{constant}$.

Now we consider the denominator in Eq. (131):

$$\frac{1}{N} \sum_{k=1}^N \log(1 + z_k^2). \quad (135)$$

As $N \rightarrow \infty$, this becomes the average of $\log(1 + z^2)$ over the distribution of site values. For any configuration we define

$$m_2 = \frac{1}{N} \sum_{k=1}^N z_k^2. \quad (136)$$

Since $\log(1 + t)$ is strictly convex for $t \geq 0$, Jensen's inequality yields $\frac{1}{N} \sum_{k=1}^N \log(1 + z_k^2) \geq \log(1 + m_2)$, with equality if and only if all z_k^2 are equal. Hence, for fixed second moment m_2 , the denominator per site is minimized by a uniform configuration.

Therefore we restrict the optimization to symmetric product states of the form

$$|\phi(\theta)\rangle = (\cos\theta |0\rangle + \sin\theta |1\rangle)^{\otimes N}, \quad 0 \leq \theta \leq \frac{\pi}{2}. \quad (137)$$

The overlap is

$$\langle\phi(\theta)|\Psi_2(q=0)\rangle\langle\phi(\theta)|\Psi_2(q=0)\rangle = \frac{\sqrt{3}}{N^2} \sum_{x_1 < x_2} (x_2 - x_1) \sin^2\theta (\cos\theta)^{N-2}. \quad (138)$$

Using translational invariance, the sum depends only on separations $r = (x_2 - x_1)$,

$$\sum_{x_1, x_2} (x_2 - x_1) = N \sum_{r=1}^{N-1} r = \frac{N^2(N-1)}{2}. \quad (139)$$

Hence, for large N ,

$$|\langle\phi(\theta)|\Psi_2(q=0)\rangle\langle\phi(\theta)|\Psi_2(q=0)\rangle|^2 = \frac{3}{4} N^2 \sin^4\theta (\cos^2\theta)^{N-2} \quad (140)$$

Maximizing Eq. (140) with respect to θ is equivalent to maximizing

$$f(\theta) = \sin^4\theta (\cos^2\theta)^{N-2}.$$

Setting $\partial_\theta \ln f(\theta) = 0$ yields

$$4 \cot\theta - 2(N-2) \tan\theta = 0, \quad (141)$$

which gives the optimal angle

$$\sin^2\theta = \frac{2}{N}, \quad \cos^2\theta = 1 - \frac{2}{N}. \quad (142)$$

Substituting Eq. (142) into Eq. (140),

$$\Lambda(|\Psi_2(q=0)\rangle) = \frac{3}{4} N^2 \left(1 - \frac{2}{N}\right)^{N-2} \times \frac{4}{N^2} = 3 \left(1 - \frac{2}{N}\right)^{N-2}. \quad (143)$$

Taking the thermodynamic limit,

$$\lim_{N \rightarrow \infty} \left(1 - \frac{2}{N}\right)^{N-2} = e^{-2}, \quad (144)$$

we obtain

$$\Lambda(|\Psi_2(q=0)\rangle) = \frac{3}{e^2}. \quad (145)$$

Therefore,

$$\lim_{N \rightarrow \infty} E_G(|\Psi_2(q=0)\rangle) = 1 - \frac{3}{e^2} \approx 0.5940. \quad (146)$$

The scaling $\sin^2\theta \sim 2/N$ reflects the two-magnon nature of the state. Compared to the generalized W state, the overlap decreases faster with N , leading to a larger geometric GME. This result is consistent with the general behavior of symmetric Dicke states with more than one excitations [11].

Geometric genuine multipartite entanglement: We consider a bipartition $A|B$ with $|A| = m$ and $|B| = N - m$. Because the state contains exactly two excitations, the reduced density matrix ρ_A decomposes into orthogonal excitation sectors

$$\rho_A = \rho_{AA} \oplus \rho_{AB} \oplus \rho_{BB}, \quad (147)$$

corresponding respectively to (a) two excitations in A , (b) one excitation in A , (c) zero excitations in A .

This block decomposition follows from particle-number conservation: sectors with different excitation numbers in subsystem A are orthogonal and therefore do not mix in ρ_A .

The traces of the outer blocks define the probabilities

$$p_{AA} = \text{tr } \rho_{AA}, \quad p_{BB} = \text{tr } \rho_{BB}, \quad (148)$$

which represent the probabilities that both magnons reside in A or both reside in B , respectively. The one-excitation block ρ_{AB} has at most two nonzero eigenvalues, which we denote by λ_1 and λ_2 .

Since the blocks act on orthogonal sectors, the spectrum of ρ_A is the union $\{p_{AA}\} \cup \{\lambda_1, \lambda_2\} \cup \{p_{BB}\}$. Therefore the largest Schmidt coefficient across any cut is

$$\lambda_{\max} = \max(p_{AA}, p_{BB}, \lambda_1, \lambda_2), \quad (149)$$

with the normalization condition

$$p_{AA} + p_{BB} + \lambda_1 + \lambda_2 = 1, \quad (150)$$

which follows from $\text{tr } \rho_A = 1$.

We now specialize to the cut where A consists of a single site. A single site cannot host two excitations simultaneously, hence

$$p_{AA} = 0. \quad (151)$$

The quantity p_{AB} corresponds to configurations in which exactly one magnon occupies site $x_1 \in A$ while the second magnon resides at some $x_2 \neq x_1$ in B . Therefore,

$$p_{AB} = \sum_{x_2 \neq x_1} \left| \frac{\sqrt{3}}{N^2} (x_2 - 1) \right|^2 = \frac{1}{4N} + \frac{1}{2N^3}. \quad (152)$$

Now, subsystem A has dimension one in the single-excitation sector, ρ_{AB} is rank one. Therefore,

$$\lambda_1 = p_{AB}, \quad \lambda_2 = 0. \quad (153)$$

The remaining probability weight lies in the zero-excitation sector:

$$p_{BB} = 1 - p_{AB}. \quad (154)$$

Thus from Eq. (149) the full spectrum of ρ_A now becomes

$$\{0, p_{AB}, 1 - p_{AB}\}. \quad (155)$$

Hence

$$\lambda_{\max} = \max(p_{AB}, 1 - p_{AB}). \quad (156)$$

From Eq. (152), in the large N limit, the dominant eigenvalue is

$$\lambda_{\max} = 1 - \frac{1}{4N} - \frac{1}{2N^3}. \quad (157)$$

Thus in the thermodynamic limit $\lambda_{\max} \rightarrow 1$, implying that the microscopic $1|N - 1$ cut dominates the maximization over all bipartitions. Using the definition of the geometric measure of GME, $E_G = 1 - \lambda_{\max}^2$, we expand perturbatively in $1/N$ and obtain

$$E_G = \frac{1}{2N} - \frac{1}{16N^2} + \mathcal{O}(N^{-3}). \quad (158)$$

Therefore the geometric GME vanishes in the thermodynamic limit, with leading finite-size correction proportional to $2/N$.

* samudra.sur@unige.ch

† author for correspondence; saikats@imsc.res.in

- [1] H. Bethe, “Zur theorie der metalle,” *Zeitschrift für Physik* **71**, 205–226 (1931).
- [2] Yu. A. Izyumov and Yu. N. Skryabin, *Statistical Mechanics of Magnetically Ordered Systems* (Springer-Verlag, Heidelberg, 1988).
- [3] Chanchal K. Majumdar, G. Mukhopadhyay, and A. K. Rajagopal, “A simple derivation of the three magnon bound state equation,” *Pramana* **1**, 135–146 (1973).
- [4] H. P. Breuer and F. Petruccione, *The theory of open quantum systems* (Oxford University Press, Great Clarendon Street, 2002).
- [5] Nikolaos E. Palaiodimopoulos, Maximilian Kiefer-Emmanouilidis, Gershon Kurizki, and David Petrosyan, “Excitation transfer in disordered spin chains with long-range exchange interactions,” *SciPost Phys. Core* **6**, 017 (2023).
- [6] M. Muraio, M. B. Plenio, S. Popescu, V. Vedral, and P. L. Knight, “Multiparticle entanglement purification protocols,” *Phys. Rev. A* **57**, R4075–R4078 (1998).
- [7] W Dur and H J Briegel, “Entanglement purification and quantum error correction,” *Reports on Progress in Physics* **70**, 1381 (2007).
- [8] W. Dur, H. Aschauer, and H.-J. Briegel, “Multiparticle entanglement purification for graph states,” *Phys. Rev. Lett.* **91**, 107903 (2003).
- [9] W. Dür, G. Vidal, and J. I. Cirac, “Three qubits can be entangled in two inequivalent ways,” *Phys. Rev. A* **62**, 062314 (2000).
- [10] Tzu-Chieh Wei and Paul M. Goldbart, “Geometric measure of entanglement and applications to bipartite and multipartite quantum states,” *Phys. Rev. A* **68**, 042307 (2003).
- [11] Robert Hübener, Matthias Kleinmann, Tzu-Chieh Wei, Carlos González-Guillén, and Otfried Gühne, “Geometric measure of entanglement for symmetric states,” *Phys. Rev. A* **80**, 032324 (2009).
- [12] T. Bastin, S. Krins, P. Mathonet, M. Godefroid, L. Lamata, and E. Solano, “Operational families of entanglement classes for symmetric n -qubit states,” *Phys. Rev. Lett.* **103**, 070503 (2009).
- [13] Tamoghna Das, Sudipto Singha Roy, Shrobona Bagchi, Avijit Misra, Aditi Sen(De), and Ujjwal Sen, “Generalized geometric measure of entanglement for multiparty mixed states,” *Phys. Rev. A* **94**, 022336 (2016).
- [14] Tzu-Chieh Wei and Simone Severini, “Matrix permanent and quantum entanglement of permutation invariant states,” *Journal of Mathematical Physics* **51**, 092203 (2010).
- [15] Philip J. Davis, *Circulant Matrices*, Pure and Applied Mathematics (John Wiley & Sons, New York, 1979).